Quantum Electronics **52** (3) 208–226 (2022)

https://doi.org/10.1070/QEL18001

Post-compression of femtosecond laser pulses using self-phase modulation: from kilowatts to petawatts in 40 years

E.A. Khazanov

Abstract. **The pulse duration at the output of femtosecond lasers is usually close to the Fourier limit, and can be shortened by increasing the spectral width. To this end, use is made of self-phase modulation when a pulse propagates in a medium with cubic nonlinearity. Then, the pulse with a chirp (frequency dependence of the spectrum phase) is compressed due to a linear dispersion element, which introduces a chirp of the same modulus, but opposite in sign. This pulse post-compression, known since the 1960s, has been widely used and is being developed up to the present for pulses with energies from fractions of a nJ to tens of J. The review is devoted to the theoretical foundations of this method, problems of energy scaling, and a discussion of the results of more than 150 experimental studies.**

Keywords: *post-compression, TFC, CafCA, femtosecond lasers, Kerr nonlinearity.*

1. Introduction

From the advent of lasers [1] to the present day, one of the main goals of research has been to obtain the shortest possible laser pulses [2]. There are three reasons why short pulses are of interest. Firstly, it is a tool for studying ultrafast processes in physics, chemistry, and biology. In this case, the laser pulse plays the role of a clock; more precisely, the duration of the pulse is equal to the division value of the clock, i.e., it determines the minimum measurable time. For pump–probe experiments, two replicas of a short pulse are used, with their energy or power being usually quite moderate. Secondly, under certain conditions, short pulses open the way to experiments that are inaccessible for longer pulses. For example, the generation of high harmonics (sequences of attosecond pulses) [3] requires femtosecond pulses, while the generation of single attosecond pulses requires pulses with a duration close to a single cycle of the electromagnetic radiation field. In such applications, in addition to a short duration, a specific, sometimes very significant, power of pulsed radiation is also needed. Thirdly, in the field of super-high power lasers [4] and superintense fields, the pulse duration also plays a key role, since the power depends only on the pulse energy and duration. An increase in the energy of such lasers is associated with an increase in the number of amplifiers, which greatly increases the already significant size and cost of lasers. Moreover, the radiation power of modern lasers is limited not by the fact that the laser pulse cannot be further amplified in CPA amplifiers [5] (CPA: Chirped Pulse Amplification), but by the fact that after amplification it cannot be compressed, since diffraction gratings have a low damage threshold , which limits the power. Thus, the only way to multiply the power of such lasers in practice is to shorten the output pulse after the diffraction grating compressor. Note that in the region of superintense fields, a short pulse duration (even at the same power) is sometimes an advantage.

The pulse duration at the output of femtosecond lasers usually slightly exceeds the Fourier limit, and for its multiple shortening one needs to increase the width of the emission spectrum by at least the same factor. To do this, self-phase modulation (SPM) of a laser pulse is used during its propagation in a medium with a cubic (Kerr) nonlinearity, whose refractive index n depends on the intensity as:

$$n = n_0 + n_2 I, \tag{1}$$

where n_0 is the linear refractive index, and n_2 is the nonlinear refractive index determined by the cubic nonlinearity tensor $\chi^{(3)}$. As can be seen from (1), the pulse in this case passes through a medium with a time-varying refractive index, since $I = I(t)$. This leads to SPM and, consequently, to the broadening of the emission spectrum:

$$\omega_{\text{inst}}(t) \equiv \frac{\partial \Phi}{\partial t} = \omega_0 - k_0 z \frac{\partial n}{\partial t}. \tag{2}$$

Here ω_{inst} and ω_0 are the instantaneous and centre frequencies; $k_0 = \omega_0/c$; $\Phi = \omega_0 t - k_0 z n$ is the phase; z is the coordinate; and c is the speed of light. Spectrum broadening is only one of the necessary conditions for the pulse shortening; in addition, it is required that all frequency components of the spectrum be in phase. At the output of a nonlinear element, the pulse becomes chirped, i.e. its instantaneous frequency (phase) becomes time-varying. In other words, the nonlinear element introduces the dependence of the phase of the spectrum on the frequency, which must be compensated for by adding the phase equal in the magnitude but opposite in sign. This is not difficult to do, since, as it is easy to see from (1) and (2), ω_{inst} near the pulse maximum depends linearly on the frequency, while the phase of the spectrum depends quadratically (see Fig. 1). Unlike nonlinear broadening of the spectrum, correction of the phase of the pulse spectrum is a linear operation, which is performed using a grating or prism compressor, chirped mirrors, liquid crystal or acousto-optic modulators,

E.A. Khazanov Institute of Applied Physics, Russian Academy of Sciences, ul. Ulyanova 46, 603950 Nizhny Novgorod, Russia; e-mail: efimkhazanov@gmail.com

Received 12 January 2022
Kvantovaya Elektronika **52** (3) 208–226 (2022)
Translated by I.A. Ulitkin

etc. Within the framework of this review, we will not consider the features of these devices, referring the reader, for example, to review [6]. This method of nonlinear compression of laser pulses (see Fig. 1) is usually called post-compression. In applications to high-power lasers, the term TFC (Thin Film Compression) [7] or CafCA (Compression after Compressor Approach) [4, 8] is used.

The idea of laser pulse compression using external phase modulation and subsequent dispersion compensation was proposed in 1968 [9] based on an analogy with pulse compression in chirped radars [10, 11]. Phase modulation in [9] was implemented using an electro-optical crystal, to which a sinusoidal voltage was applied. The laser pulse passed through the crystal at the moment of the zero phase of the voltage, i.e., the pulse frequency changed linearly in time. Duguay and Hansen [12] not only chirped a 500-ps pulse in an electro-optical crystal, but also compressed it to 270 ps using a Gires–Tournois interferometer [13].

The key idea – use of cubic nonlinearity for SPM – was proposed by Fisher et al. [14] in 1969. In this work, they theoretically substantiated the method and demonstrated the prospects of using the CS_2 liquid as a nonlinear medium and the Kerr effect as a nonlinear effect. In the same year, Laubereau [15] experimentally implemented nonlinear compression: a 20-ps pulse was compressed several times. A significant drawback of the liquid is the long relaxation time of the Kerr nonlinearity (2 ps for CS_2), which limits the pulse duration to the picosecond range. Apparently, for this reason, the idea was 'forgotten' and reincarnated only in the 1980s with the development of femtosecond lasers and fibre technology.

Post-compression is the subject of several reviews [2, 6, 8, 16, 17] focused on certain methods of its implementation and the corresponding ranges of pulse intensity. The purpose of this review is to summarise the main experimental results obtained over the past 40 years in the field of nonlinear compression of femtosecond laser pulses. The review is organised as follows. Section 2 briefly discusses the physical foundations of SPM and the limitations that arise when the input pulse power is increased. A detailed review of the results for all variants of the geometry of a nonlinear medium is given in Sections 3 and 4 for waveguide and free propagation, respectively. For scaling the compressed pulse power, the suppression of small-scale self-focusing is of fundamental importance. Section 5 is devoted to this problem.

2. Theoretical foundations of self-phase modulation and post-compression

A plethora of works are devoted to the physics of self-phase modulation and pulse post-compression. In this review, we will focus on experimental papers (Sections 3 and 4), and in this section we will restrict ourselves to a brief listing of the main equations, and input and output parameters of the problem (Section 2.1), as well as to a discussion of the limitations and problems that arise in the scaling of the power (Section 2.2).

2.1. Equation, problem parameters, pulse compression factor

Propagation of laser pulses in a medium with a Kerr nonlinearity is given in the approximation of slowly varying amplitudes by the generalised nonlinear Schrödinger equation, the linear part of which describes diffraction, dispersion, spatiotemporal focusing, and linear losses, and the nonlinear part describes the instantaneous Kerr nonlinearity, retarded (Raman) nonlinearity, and also plasma nonlinearity: ionisation by a laser field and the influence of the resulting plasma on diffraction and dispersion. In full form [18–21], the equation is cumbersome, and therefore we present it in a simplified form, in which all orders of dispersion (important only for very short pulses) except the second one, linear losses (a parasitic effect that needs to be minimised), and also the Raman and plasma nonlinearities are neglected. These nonlinearities (along with the instantaneous Kerr nonlinearity) can be used for pulse compression, which, however, is beyond the scope of this review.

It is convenient to write the equation by normalising the coordinates z and r, the time t, and the electric field amplitude E to the corresponding radiation parameters at $z = 0$ and to the nonlinear medium length L:

$$\xi = \frac{z}{L},\ \eta = \frac{t - z/u}{T_{\text{in}}},\ r_\perp = \frac{r}{w},\ \Psi = \frac{E}{E_{\text{in}}}, \tag{3}$$

where u is the group velocity at a frequency $\omega = \omega_0$; E_{in} is the input field intensity maximum in time and space; and T_{in} and w are the pulse duration and beam radius at the entrance, respectively. Here we will not specify the shape of the pulse and the shape of the beam (in a large number of cases they are close to Gaussian). Taking into account (3), the equation for Ψ has the form

$$\frac{\partial}{\partial\xi}\Psi - D\frac{\mathrm{i}}{2}\frac{\partial^2}{\partial\eta^2}\Psi - Z\frac{\mathrm{i}}{2}\left(1 + \frac{\mathrm{i}}{2\pi N}\frac{\partial}{\partial\eta}\right)^{-1}\Delta_\perp\Psi = -\mathrm{i}B\left(1 + \frac{\mathrm{i}}{2\pi N}\frac{\partial}{\partial\eta}\right)|\Psi|^2\Psi, \tag{4}$$

which shows that the problem is determined by four dimensionless parameters:

$$N = T_{\text{in}}\frac{c}{\lambda}, \tag{5}$$

$$D = L\frac{k_2}{T_{\text{in}}^2}, \tag{6}$$

$$Z = \frac{L}{n_0 k_0 w^2}, \tag{7}$$

$$B = k_0 n_2 I_{\text{in}} L. \tag{8}$$

Here $k_2 = \partial^2 k n_0(\omega)/\partial\omega^2$ is the group velocity dispersion, and I_{in} is the maximum intensity in time and space at $z = 0$. These four parameters have a simple physical meaning: N is the number of field cycles in the input pulse; D is the ratio of L to the dispersion length $L_{\text{d}} = T_{\text{in}}^2/k_2$; Z is the ratio of L to the Rayleigh length $L_{\text{R}} = n_0 k_0 w^2$; and the parameter B is the B-integral or nonlinear phase. Strictly speaking, the nonlinear phase incursion, as is easy to see from (1), is determined by the expression

$$\Phi_{\text{nl}} = k_0\int_0^L n_2 I \mathrm{d}z, \tag{9}$$

and $\Phi_{nl} \neq B$ if the pulse intensity changes during propagation (even for $n_2 = \text{const}$). However, as a rule, it is the parameter B that is used in experimental work, since it has two important advantages: B is determined only by the conditions of the problem and can be easily measured. On the contrary, in order to find Φ_{nl}, it is necessary to solve equation (4), while Φ_{nl} is very difficult to measure.

In most cases, the ultimate goal of post-compression is to increase the pulse power $F_p = P_{out}/P_{in}$ or even increase the intensity in the focal plane. At the same time, most experimental works measure the pulse compression factor

$$F = T_{in}/T_{out}, \tag{10}$$

with T_{in} and T_{out} being the full width at half maximum (FWHM) pulse duration. The parameter F is always greater than F_p, both due to energy losses and due to the transfer of part of the energy to the pulse periphery, which does not change T_{out}, but reduces P_{out}. Below we will discuss exactly the pulse compression factor F as a post-compression criterion, as well as P_{out} and T_{out}.

The parameter Z is responsible for the beam diffraction and does not directly affect the pulse compression during collinear propagation; however, as will be discussed in detail below, it is the spatial effects that limit the pulse power scaling. Numerical simulation (4) shows that for long pulses ($N \gg 1$), the value of N does not significantly affect the compression. Nevertheless, for short pulses, the last term on the right-hand side of (4) leads to a 'self-steepening' of the pulse front and to the formation of an envelope shock wave. This circumstance was first pointed out in [22] and later in [23, 24]. Note that Anderson and Lisak [25] found an analytical solution to (4), neglecting dispersion ($D = 0$) and diffraction ($\Delta_\perp = 0$).

The influence of the parameter D depends on its value and sign; more precisely, the relation between the signs of D and B is important, i.e., between the signs of k_2 and n_2. As a rule, the signs of k_2 and n_2 are positive for transparent dielectrics in the visible and near-IR ranges. If the signs are opposite, then self-compression is possible during propagation in the medium. In this review, we will not consider self-compression; we refer the reader, for example, to papers [26–30]. The authors of Ref. [8] analysed the influence of the value of D both on the broadening of the spectrum and on the compression factors F and the increase in power F_p. They showed that for a Gaussian pulse at $D < 0.05$, F can be estimated with high accuracy by the formula

$$F = 1 + 0.59B(1 - 1.26\sqrt{D}). \tag{11}$$

As can be seen from (11), dispersion reduces F, and its role can be interpreted as a decrease in the effective value of the B-integral by a factor of $1-1.26D^{1/2}$. Paper [8] also showed that the factor F_p is less affected by dispersion than F: for example, at $B = 20$, the factor F_p at $D = 0.05$ is only 1.2 times less than F_p at $D = 0$, while F is 1.7 times less. These calculations were made by correcting the quadratic component of the spectrum phase. If a full correction is applied, i.e., the phase of the output pulse is set constant, then F will be larger, but insignificantly, by 10%. Numerical simulation at $B = 48$ showed [31] that even for such an extreme value of the B-integral, F is only 20% less than that which follows from (11). Thus, of the four parameters in (4), the B-integral is the determining one. The remaining parameters and the effects behind them are rather parasitic in nature, defining the limitations and problems that arise during post-compression.

In conclusion, we note that SPM is studied numerically without the approximation of slowly varying amplitudes (see, for example, [32–34]).

2.2. Post-compression power scaling limitations

Four main problems can be formulated that limit the power scaling of both the input and output pulses: large-scale self-focusing, small-scale self-focusing, optical breakdown of the medium, and spatial inhomogeneity of SPM.

2.2.1. Large-scale self-focusing (LSSF). Large-scale self-focusing – self-focusing of the beam as a whole – occurs if the beam power exceeds the critical self-focusing power P_{cr}. Physically, P_{cr} denotes the power at which the diffraction spreading of the beam is compensated for by self-focusing. In particular, for $P_{in} = P_{cr}$, the beam size at the focus of a conventional lens tends to zero if the beam has a plane wavefront in front of the lens. For $P_{in} > P_{cr}$, collapse is possible even without a lens. However, the condition $P > P_{cr}$ and even $P \gg P_{cr}$ does not imply that the collapse is inevitable, because collapse requires a certain length of beam propagation in a nonlinear medium, L_{cr}. Goldberg et al. [35] found numerically the values of P_{cr} and L_{cr} for a Gaussian beam:

$$P_{cr} = \frac{0.174\lambda^2}{n_2 n_0}, \tag{12}$$

$$L_{cr} = \frac{0.37 k_0 n_0 w^2}{\sqrt{(\sqrt{P/P_{cr}} - 0.825)^2 - 0.03}}, \tag{13}$$

where w is the beam radius (according to the intensity level 1/e). In other works, for example, in [36], the numerical coefficients in these formulae are slightly different, but this difference is not fundamental for us. The parameter P_{cr} is almost completely determined by n_2. Typical values of P_{cr} in solids are several MW, while in gases at atmospheric pressure they are three to four orders of magnitude higher. This circumstance determines the advantage of gases (see Section 3 for details). It is of fundamental importance that the key parameter is precisely the power, rather than the intensity, i.e., P_{cr} does not depend on the beam radius w. On the contrary, L_{cr} grows quadratically with w. In addition, L_{cr} at $P \gg P_{cr}$ is proportional to $(P_{cr}/P)^{0.5}$, which was first pointed out by Kelly [37]. This causes a common misconception that LSSF is the most dangerous for high-power lasers. In fact, the opposite is true because LSSF does not pose any danger to high-power lasers because of the large beam sizes. Substituting $P = \pi w^2 I$ into (13), for $P \gg P_{cr}$ we obtain

$$\frac{L_{cr}}{L} = \frac{1.4}{\sqrt{Bn_0}} \frac{w}{\sqrt{L\lambda}}. \tag{14}$$

Taking into account the fact that in high-power lasers L is on the order of a millimetre, for beams with $w > 1$ mm we obtain $L_{cr} \gg L$, i.e., LSSF is excluded. In other words, the collapse is not only absent in a nonlinear medium, but also the beam diameter remains virtually unchanged.

2.2.2. Small-scale self-focusing (SSSF). The instability of a plane wave propagating in a medium with a cubic nonlinearity [38] leads to an increase in spatial perturbations and, as

a consequence, to small-scale self-focusing (SSSF). Due to SSSF, the beam is split into many filaments, which significantly degrades the beam quality and, finally, leads to the breakdown of optical elements. Each filament contains a power of the order P_{cr}, i.e., SSSF is possible only for $P > P_{cr}$. The development of SSSF is determined both by disturbances (noise) at the input to the medium and by the nonlinearity itself. On the one hand, the power and spatial noise spectrum are quite difficult to measure in practice, and on the other hand, their influence on SSSF is not so great, since they serve only as a seed. The gain of these noises depends on the angle θ between the perturbation wave vector and the z axis, as well as on the B-integral. The gain is maximum at

$$\theta = \theta_{max} = \sqrt{\frac{2n_2 I_{in}}{n_0}} \tag{15}$$

and is approximately equal to unity at $\theta > 2^{1/2}\theta_{max}$. For the most dangerous angles $\theta \approx \theta_{max}$, the gain depends exponentially on B, and so B is the main parameter that determines the presence or absence of SSSF. Unlike LSSF, for SSSF it is not power that is important, but intensity. The similarity lies in the fact that the medium length L is important: even at large I_{in}, the B-integral can be small for a short medium. The stationary theory of SSSF has been described in many papers (see, for example, [8, 38–42]. In the stationary case, the beam of nanosecond lasers is split into filaments, as a rule, at $B > 2–3$; therefore, the analogue of L_{cr} for SSSF is length at which $B = 3$. Thus, not only the same nonlinearity, but also the same parameter – the B-integral – is both useful and parasitic for compression (11). At first glance, post-compression is possible only in a narrow range, $B < 3$, which even theoretically (11) makes it possible to expect insignificant pulse compression, but this is not the case, since high-power femtosecond lasers have two significant differences from nanosecond lasers.

The first difference is spatial. A fundamentally important feature of SSSF in high-power femtosecond lasers compared to nanosecond lasers is a significant increase in θ_{max}. This is due to the fact that the breakdown threshold of optical elements in the femtosecond range is much higher and the laser radiation intensity I_{in} equals not units of GW cm^{-2}, but units of TW cm^{-2}, and, consequently, θ_{max} increases by a factor of 30. The second difference is spatiotemporal. It requires taking into account linear dispersion, nonlinear dispersion, and the fact that during propagation the perturbation can lag behind the main pulse, and if the delay time is comparable with the pulse duration, then the instability is suppressed. These differences make it possible, under certain conditions, to avoid SSSF and implement post-compression even for $B \gg 3$. We will discuss this in more detail in Section 5.

2.2.3. Optical breakdown of the medium. At a high intensity of the laser beam, ionisation of a nonlinear medium is possible, which results in plasma generation. In some cases, this is a positive effect, which is used, among other things, for SPM and subsequent compression. In this case, the nonlinear refractive index is no longer proportional to the intensity (1), since it is determined by the plasma density. Because the plasma density always increases with time (in contrast to intensity), the instantaneous frequency changes monotonically [see (2)], shifting all the time to the short-wavelength region (blue-shift). Accordingly, the chirp is very different from the linear one, which makes subsequent compression difficult. Nevertheless, compression based on ionisation nonlinearity is possible, even in the filamentation regime. However, its consideration is beyond the scope of this review; therefore, we confine ourselves to references to reviews [19, 43] and further consider ionisation and optical breakdown as parasitic effects that must be avoided.

Ionisation is determined by the intensity of the radiation beam, the threshold value of which I_{br} is approximately 10^{13} W cm^{-2} for solids and $10^{14}–10^{15}$ W cm^{-2} for noble gases. Thus, the power P_{in} is strictly limited by $P_{br} = \pi w^2 I_{br}$, i.e., it depends quadratically on the beam radius. Unlike LSSF and SSSF, the limitation does not depend on the medium length L; moreover, for solids, I_{br} on the surface is usually lower than in the bulk.

2.2.4. Spatial inhomogeneity of SPM. Because the beam intensity depends on the transverse coordinate r, then in the general case both the B-integral (8) and the nonlinear phase (9) are functions of r. This leads to two undesirable consequences. First, a pulse is compressed inhomogeneously in r: the compression factor F (11) depends on B. In particular, at the beam periphery, where the intensity is much lower than on the axis, the compression effect practically disappears. Second, the spatial inhomogeneity of the phase leads to nonlinear distortions of the wavefront, which deteriorates the quality of beam focusing, reducing the focal intensity. Both of these consequences can significantly reduce the benefit of pulse compression.

At small values of B, the inhomogeneity is also insignificant, but large values of the compression factor F require large B. Thus, the spatial inhomogeneity of SPM is determined by the B-integral and the shape of the beam (obviously, inhomogeneity is absent for a flat-top beam, and for a super-Gaussian beam it is less than that for a Gaussian beam). Post-compression of low-power pulses is based on waveguide propagation (see Section 3), in which this effect is absent: the entire spatial mode acquires a nonlinear phase, and there is no dependence of the phase on r. High power requires the rejection of waveguides, and the problem of the spatial inhomogeneity of SPM comes to the fore (see Section 4).

It is obvious that the influence of the above-considered four restrictions on the power scaling during post-compression essentially depends on the geometry of beam propagation in a nonlinear medium (see Fig. 1). In Sections 3 and 4, we consider all known variants of the geometry and determine which of the restrictions are dramatic and which are insignificant, as well as present a review of the experimental results.

3. Waveguide propagation

Figure 1 schematically shows eight variants for the geometry of a nonlinear medium. First of all, it is necessary to separate the waveguide and free propagation of the beam. In the first case, it is needed to form at the input a beam that is as close as possible to the mode (usually the lowest) of the corresponding waveguide. In an ideal case, the same mode will be at the output, the pulse energy will be conserved, and SPM will appear. If there is an intermode interaction, then part of the energy will be transferred to other modes, which, as a rule, are emitted from the waveguide, leading to an energy loss. The main disadvantage of waveguides is the small size of the mode, which limits the power. Their undoubted advantage is their

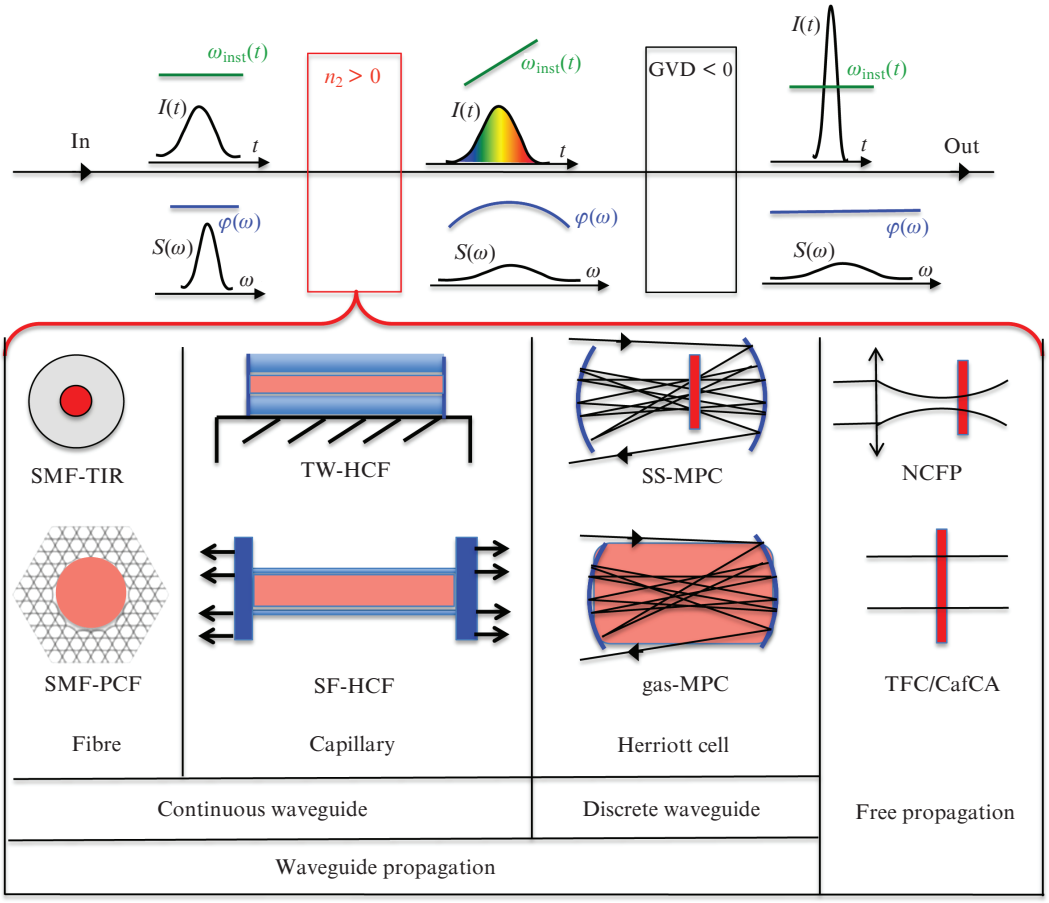

Figure 1. (Colour online) Principle of post-compression and variants of the geometry of a nonlinear medium.
SMF-TIR is a single-mode fibre based on total internal reflection; SMF-PCF is a single-mode fibre with a microstructured cladding, the so-called photonic crystal fibre; TW-HCF is a gas filled rigid thick walled hollow-core fibre; SF-HCF is a gas-filled thin walled stretched flexible hollow-core fibre; SS-MPC is a solid-state-based Herriott multipass cell; gas-MPC is a gas-filled Herriott multipass cell; NCFP is noncollinear free propagation of a focused beam; TFC/CafCA (Thin Film Compression/Compression after Compressor Approach) is free propagation of a collimated beam; and $S(\omega)$ and $\varphi(\omega)$ are the amplitude and phase of the Fourier spectrum of the pulse.

large length, which provides a large B-integral even at a low intensity.

3.1. Single mode fibre (SMF)

The simplest waveguide is a single-mode fibre (SMF), in which the field is retained due to either total internal reflection (SMF-TIR: Single Mode Fibre – Total Internal Reflection) or cladding microstructuring – the so-called photonic crystal fibres (SMF-PCF: Single Mode Fibre–Photonic Crystal Fibre). Note the minimum energy loss, as well as compactness and practically unlimited length, which makes fibres indispensable for low-power lasers. At the same time, a very small aperture of single-mode fibres is also their main disadvantage: LSSF and optical breakdown limit power scaling. In SMF-TIR, the input power P_{in} is strictly limited to $P_{cr} \approx 4$ MW, since L_{cr} is small due to the small diameter. The value of P_{br}, although insignificantly, is greater than P_{cr}; therefore, single-mode fibres, even with a large aperture, do not allow the power P_{in} to be increased to a value exceeding P_{cr}.

Significant progress in this direction is associated with single-mode photonic crystal fibres created in 1996 [44]. First, the size of the fundamental mode in SMF-PCFs is increased (while maintaining single-mode propagation) due to the fact that the high modes are not held by the structure surrounding the core of the fibre. However, this in itself does not lead to significant power scaling, since the main limitation, P_{cr}, does not depend on the aperture (12). This limitation was overcome by hollow-core SMF-PCFs [45], in which P_{cr} is much higher, since light propagates mainly through air or another gas, i.e., in a medium whose P_{cr} is several orders of magnitude higher than that of fused silica. Thus, optical breakdown limits the power. The threshold breakdown power P_{br} in hollow-core SMF-PCFs is higher due to both the higher (compared to silica) gas breakdown threshold and the large mode size (up to 100 μm or greater) [46]. An increase in the fibre mode size is discussed in detail in [47]. Another important advantage of hollow-core PCFs is their wide bandwidth. The properties of PCFs are described in detail in review [48]. The results of experiments with SMF-TIR [49–69] (Sections 3.1.1) and with SMF-PCF [70–89] (Sections 3.1.2) are presented in Fig. 2 in historical development and in Figs 3 and 4 on the parameter plane.

3.1.1. Fibre based on total internal reflection (SMF-TIR). Spectrum broadening in SMF-TIR was first demonstrated by Stolen and Lin [90], with the maximum value of the B-integral

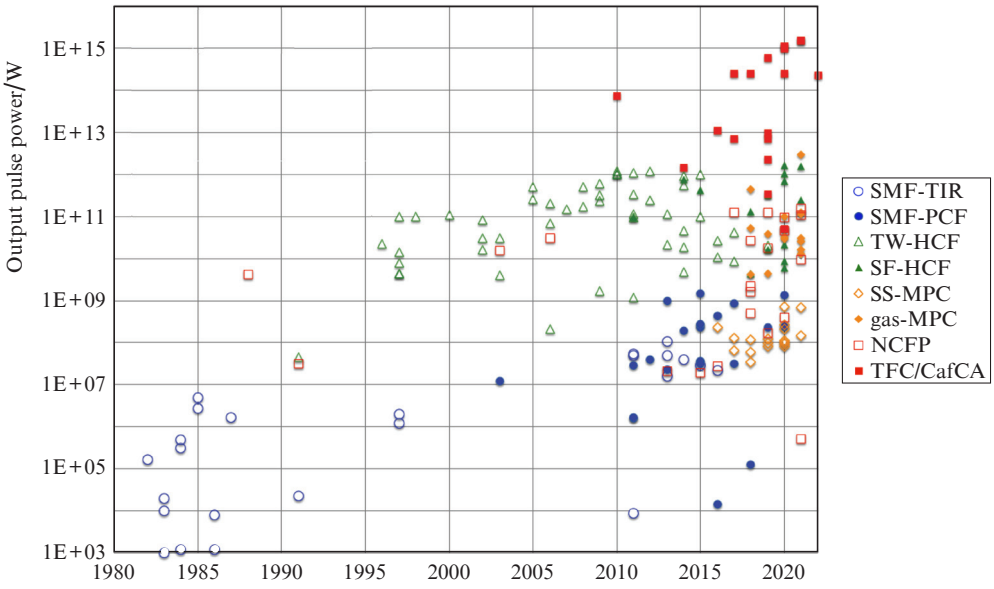

Figure 2. (Colour online) History of post-compression. Output pulse powers achieved using SMF-TIR [49–69] and SMF-PCF [70–89], TW-HCF [98, 100, 106, 108–146] and SF-HCF [14–159], Herriott SS-MPC [176–187] and gas-MPC [125, 188–200], as well as using noncollinear free propagation (NCFP) of focused [83, 51, 182, 186, 216–229] and collimated (TFC/CafCA) [230–246] beams.

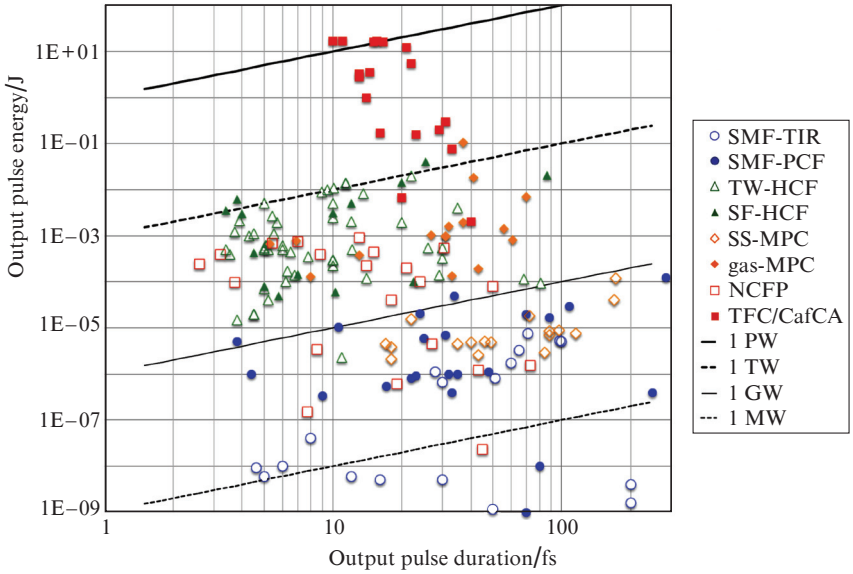

Figure 3. (Colour online) Experimental results on the 'output pulse duration – output pulse energy' plane obtained using SMF-TIR [49–69] and SMF-PCF [70–89], TW-HCF [98, 100, 106, 108–146] and SF-HCF [147–159], Herriot SS-MPC [176–187] and gas-MPC [125, 188–200], as well as using noncollinear free propagation (NCFP) of focused [83, 151, 182, 186, 216–229] and collimated (TFC/CafCA) [230–246] beams.

being 4.5π. In the same work, a detailed theoretical analysis is presented, but the issue of subsequent compression is not discussed there. Soon several theoretical papers [91–93] devoted specifically to compression appeared. The pulse was experimentally compressed for the first time in 1981 [49] (from 5.5 to 1.5 ps) using a 70-m-long single-mode fibre and a cuvette with sodium vapour used as a compressor. In the next experiment [50], compression was already carried out in the femtosecond range: a pulse with a duration T_{in} = 90 fs and an energy of several nJ was focused into a 15-cm-long fibre, after which a diffraction grating compressor compressed it to T_{out} = 30 fs.

In the 1980s and 1990s there appeared many experimental works [51–61, 94], and impressive results were immediately obtained. In particular, already in 1983, two-stage pulse compression was demonstrated [52], and in 1984 [94], a record-breaking and still unsurpassed 80-fold pulse compression per pass was demonstrated (T_{in} = 33 ps, T_{out} = 0.41 ps). In [55], a gradient fibre with a large mode diameter was used. The output pulse power P_{out} reached several MW [53, 56] and T_{out} = 6 fs [58], which for several years was the world record for the pulse duration. Note that in this work the intensity in the fibre was 1–2 TW cm^{-2}, the fibre length was only 9 mm, and two compressors (diffraction grating

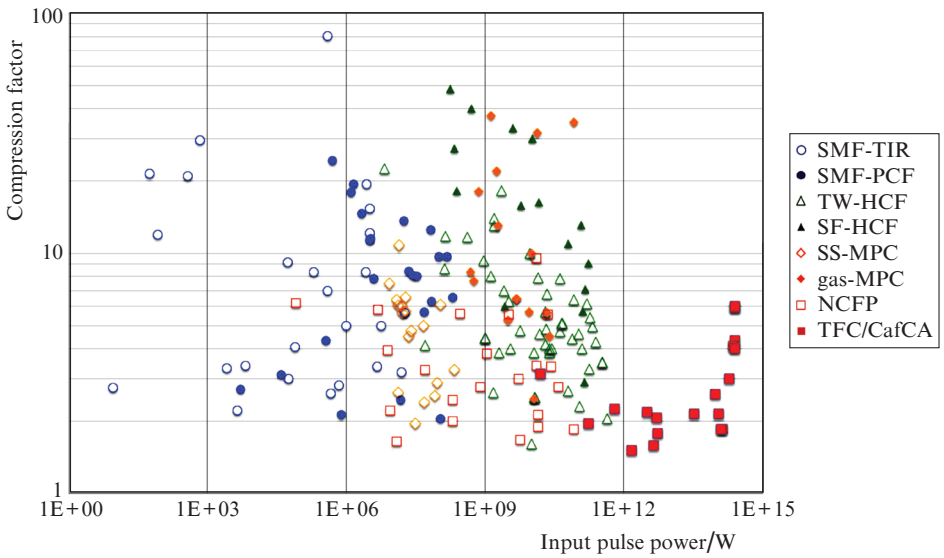

Figure 4. (Colour online) Experimental results on the 'input pulse power – compression factor' plane obtained using SMF-TIR [49–69] and SMF-PCF [70–89], TW-HCF [98, 100, 106, 108–146] and SF-HCF [147–159], Herriot SS-MPC [176–187] and gas-MPC [125, 188–200], as well as using noncollinear free propagation (NCFP) of focused [83, 151, 182, 186, 216–229] and collimated (TFC/CafCA) [230–246] beams.

and prism compressor) were used for pulse shortening. The record was broken 10 years later [60]: a pulse with a duration T_{out} = 4.6 fs even today is the shortest pulse obtained using SMF-TIR.

In the 2010s research continued, and the main effort was directed towards increasing the power output. It was increased by an order of magnitude – up to tens of MW. In [65], the input power P_{in}, although slightly, still exceeded P_{cr}. The authors do not discuss the reasons for the lack of self-focusing, but apparently this was due to the fact that a fibre with a diameter of 59 μm and a length L of only 29 mm was used, which is less than L_{cr} (12). It is possible that further optimisation of the fibre and input pulse parameters will make it possible to obtain an output power of more than 100 MW.

It is important to note that SMF-TIRs have two important advantages. First, they can be doped and used simultaneously as amplifiers [62, 67]. Second, they make it relatively easy to increase the output power by summing parallel spatial channels [66], consecutive time channels [69], or both [64]. In the latter case, 32 pulse replicas (16 temporal replicas due to the use of four birefringent crystals and two spatial replicas due to the use of a Sagnac interferometer) with a duration T_{in} = 400 fs were compressed into a single pulse with T_{out} = 71 fs and an energy of 7.5 μJ. The obtained power $P_{out} \sim$ 100 MW is a record for SFM-TIR, despite the fact that the power of each replica in the fibre was significantly less than P_{cr}.

To conclude this section, we mention the method for summing parallel channels, based on the nonlinear interaction between pulses propagating in closely spaced fibres [95]. Under certain conditions, a stable supermode is formed in such a spatial fibre grating, which automatically ensures the phasing of channels, and their number can be very large. Such a supermode was experimentally demonstrated for 25 fibres [96]. The use of this supermode for SPM and subsequent pulse compression can significantly increase the output power in the future.

3.1.2. Photonic crystal fibre (SMF-PCF). In 2004 Konorov et al. [97] demonstrated for the first time SPM in hollow-core SMF-PCFs filled with air and helium. At the same time, the first compression was demonstrated in 'conventional' (not hollow) fibres in 2003 [84], with the 33-fs pulse power P_{out} being 12 MW, and the compression factor F = 24 being a record for SMF-PCFs. Subsequent experiments with non-hollow-core SMF-PCFs [77, 80, 81] only slightly improved the results: T_{out} = 23 fs, and P_{out} = 34 MW [77], after which the attention of researchers switched to hollow-core fibres. In the first experiment [89], P_{out} was slightly more than 1 MW, while F was only 4.3. However, to date, hollow-core SMF-PCFs have significantly 'overtaken' SMF-TIRs: P_{out} has reached 1.5 GW [74], and T_{out} = 4.4 fs [76].

In [72, 75], two-stage compression was demonstrated, with the pulse self-compression occurring in the second stage due to anomalous dispersion. Note that after self-compression, both studies used additional external compression. In [71, 75], a single-ring SMF-PCF was used, which is a ring of thin-walled capillaries around a hollow core. It is also interesting to note paper [88], in which radiation pulses compressed from T_{in} = 190 fs to T_{out} = 70–120 fs were obtained, tunable in wavelength from 825 to 1210 nm.

In all experiments with SMF-TIR, P_{in} was below P_{br}, which leaves room for a further increase in power, however, the 'margin' is small and exceeding the barrier of 10 GW seems unlikely. This requires a significant increase in the aperture, i.e., a transition to hollow capillaries.

3.2. Hollow-core fibres

One can significantly increase P_{in} by abandoning single-mode fibre in favour of gas-filled capillaries, i.e. hollow-core fibres (HCFs). The principal feature of a capillary is its multimode nature, and also the fact that it is the grazing angles of incidence on the walls of the capillary rather than the total internal reflection that prevents the beam from transverse spreading. Both of these circumstances are significant drawbacks. The first requires a very precise input of radiation into the capillary and matching with the size of the fundamental

mode. The second is a high degree of straightness of the capillary, since the slightest bend leads to the emission of the fundamental mode. As a result, the energy transmission of HCFs is typically less than 50%. Advantages of HCFs are the large aperture and the use of gas as a nonlinear medium. A large aperture (up to 1 mm) and a high gas breakdown threshold increase P_{br}, while a small n_2 in gases increases P_{cr}. Moreover, using different gases and their different pressures, it is convenient to control both the nonlinearity and the dispersion over a very wide range.

It is noted in the literature that the idea of using HCFs was proposed and implemented by Nisoli and Silversti [98] in 1996. Strictly speaking, what is new in this work is the proposal to fill the capillary with a gas, and the very idea of using a capillary for SPM was realised as early as 1974 [99]. In 1991 Zhou et al. [100] demonstrated a pulse compression from 45 to 2 ps at a compressed pulse energy of 0.3 mJ. In these works, the capillary was filled with a liquid (CS_2).

Theoretical aspects of compression in HCFs can be found in [101], as well as in review [6]. Since the main power limitation is P_{cr}, we note that several papers [2, 6, 102, 103] stated that the value of P_{cr} in HCFs is greater than in free space. However, Fibich and Gaeta [104] showed that this is not the case. Usually, one tries to exclude ionisation by limiting the input intensity, but the opposite strategy is also possible, i.e. to use ionisation nonlinearity [105]. The propagation of an arbitrarily polarised beam is analysed in detail in Refs [6, 106].

The length of a conventional rigid thick walled hollow-core fibre (TW-HCF) does not exceed 1 m, since it is impossible to ensure the required quality of the inner wall at longer lengths. The fact is that losses are significant even with minimal bends (distortions) of the core. A stretched flexible thin walled hollow core fibre (SF-HCF) can have a significantly longer length. The idea [107] is that hollow cores with thin walls (tens of microns) are flexible, and this allows them to be stretched by applying opposite forces to both ends. In this way, the straightness of the hollow core is achieved (like that of a guitar string). Due to gravity, the radius of curvature R is not equal to infinity, but can reach several kilometres [107] with a moderate tensile force T, since $R = T/\rho$, where ρ is the linear density. Due to thin walls, ρ is usually less than 1 g m^{-1} [16]. It is important that R is independent of the capillary length, and hence it is limited only by the size of the laboratory.

Thus, the capillaries have radically shifted the power limits (P_{cr} and P_{br}) – up to tens of GW. Section 3.2.1 is devoted to ordinary thick-walled hollow fibres (TW-HCFs), and Section 3.2.2 describes stretched flexible hollow-cores fibres (SF-HCF) that have been actively used in recent years. The results of experiments with TW-HCFs [98, 100, 106, 108–146] and SF-HCFs [147–159] are presented in Figs 2–4.

3.2.1 Thick walled hollow-core fibres (TW-HCFs). In the very first experimental work with TW-HCFs [98], the authors managed to obtain impressive results: the pulse was compressed by a factor of 14 (from 140 to 10 fs) after passing through a capillary 70 cm long and 140 μm in diameter, filled with krypton at a pressure of 2 atm, and a compressor consisting of a pair of prisms. The output pulse power P_{out} was 22 GW, which even today is an order of magnitude higher than that achieved with the use of fibre nonlinear compressors. The next year, P_{out} = 100 GW [108] was achieved, a result that was soon repeated by the inventors of HCFs [111, 112]. In 2005, P_{out} = 0.5 TW was obtained [115], and, finally, the threshold of 1 TW was overcome in 2010 [128, 129, 146], but so far no progress has been made. The authors of Refs [127, 133, 160] obtained a slightly higher power, P_{out} = 1.2 TW, using the ionisation nonlinearity. The record duration T_{out} = 3.4 fs [120] was reached even faster, and the record compression ratio F = 18 [144] is only slightly higher than that obtained in [98] and even lower than that obtained in [100] in the picosecond range.

Further power growth in TW-HCFs is limited by LSSF: P_{cr} for argon at atmospheric pressure is about 10 GW, and for P_{out} = 1 TW to be reached, an input power P_{in} of at least 100 GW is needed. For such a radical increase in P_{cr}, neon and even helium [129] were used, which have a much smaller n_2. In addition, the idea of a longitudinal pressure gradient proposed in Refs [161, 162] played an important role: a minimum (almost zero) pressure at the input to the capillary and a maximum at the output. When propagating through a capillary, the power of pulsed radiation decreases due to the 'emission' of higher spatial modes and dispersion spreading, and, therefore, the input power can be greater than the critical power corresponding to the maximum pressure. This idea was first implemented in the above-mentioned papers with record-breaking results [115, 129], as well as in many others [116–118, 121, 124, 135, 138, 149].

It is possible to increase P_{cr} by 1/3 by using circularly polarised radiation instead of linearly polarised one, which was implemented in Refs [106, 130, 163]. Another idea for increasing P_{out} – using a planar (one-dimensional) rather than a circular capillary – was proposed in [164] and relaised in several papers [122, 123, 128, 137, 146]. This also made it possible to achieve a power P_{out} no higher than 1 TW [128, 146].

The reason for the limitation of P_{out} is related to the fact that a small value of n_2 automatically leads to a decrease in the B-integral (8) and, consequently, to a decrease in the compression factor (11). It is no coincidence that the maximum compression factor in works with terawatt power is only 6.2 [141]. The intensity is limited by the breakdown threshold, and so the B-integral can be increased only at the expense of the length. The length of rigid TW-HCFs is limited to 1 m, since the scattering into higher spatial modes is significant even with minimal bends. Stretched flexible thin walled HCFs can be much longer.

3.2.2. Stretched flexible thin walled hollow-core fibres (SF-HCFs). Already in the first work using SF-HCFs [147], a power of 93 GW was obtained in 2011, and 750 GW three years later [148]. SF-HCFs have replaced conventional TW-HCFs since 2018, and P_{out} = 1.6 TW [155, 158], a pulse duration T_{out} = 3.4 fs [154], and F = 48 [156] have been achieved. Note that the values of the first two parameters are comparable to the record values for TW-HCFs, and F is much larger. In [155, 158], use was made of capillaries with lengths of 3.75 and 3 m and diameters of 0.53 and 1 mm, filled with gases with a large P_{cr} value – helium and neon at a pressure of 2 and 2.1 atm, respectively. The maximum length of SF-HCFs to date is 6 m [150, 153]; however, in these works, the input power was low, and so argon was employed. Thus, the use of SF-HCFs has a potential to advance into the multiterawatt power range.

Although the Raman nonlinearity is beyond the scope of this review, we note work [156], in which an SF-HCF 3.5 m long and 0.5 mm in diameter was filled with molecular gases with linear N_2 or N_2O molecules, as well as argon (for comparison). Use was made of a long input pulse (T_{in} = 280 fs), for which the rotational nonlinearity is almost instantaneous.

As a result, a supercontinuum was generated with a symmetric (in contrast to the case when argon was used) spectrum of much greater width (also compared to argon). The experiments were performed with 0.4 mJ pulses, and so P_{out} did not exceed 20 GW, but the compression ratios were impressive: $F = 40$ with N_2 and $F = 27$ with N_2O. In a nitrogen-filled SF-HCF 5.5 m long and 1 mm in diameter, the power $P_{out} =$ 0.7 TW (14 mJ, 20 fs) was obtained in [157].

3.3. Discrete waveguides – Herriott multipass cells (MPCs)

Instead of continuous waveguides – fibres or capillaries – discrete ones can be employed. The beam propagates in free space, and diffraction is compensated for by periodically located lenses or mirrors, between which there are waists. This idea was proposed in [165, 166]. The authors performed detailed analytical and numerical studies showing that the compression factor F can be greater than 15 if $B < 1.6$ in each nonlinear medium. In practice, it is convenient to organise discrete waveguides using a compact Herriott cell [167], which consists of two spherical mirrors with an aperture much larger than the beam aperture. A misaligned beam is multiply reflected from the mirrors, each time passing through the waist located between them. The properties of the Herriott cell are described in more detail, for example, in [168]. Such devices are called multipass cells (MPCs): the radiation passes through them dozens of times. As a nonlinear medium, use is made of both solid-state plates, usually located near the waist [solid-state-based multipass cells (SS-MPCs)], and a gas that fills the cell completely [gas-filled multipass cells (gas-MPCs)]. In both cases, SPM, while remaining small per pass, accumulates per many passes. In SS-MPCs, light propagates most of the way in a linear medium, while the nonlinear medium is thin and its length can be less than L_{cr}. This makes it possible to use the pulse power P_{in} higher than P_{cr}, and at the same time avoid LSSF (see Section 2.2.1). A detailed theoretical study can be found in [169] and in patent [170].

The use of gas-MPCs for SPM was proposed in [169]. There are two qualitative differences from the case of using SS-MPCs. First, the nonlinear medium occupies the entire propagation region, i.e., the length of the medium is much longer than the waist length: $L \gg kw^2$. In his pioneering work Talanov [171] found a change in variables that allows one to solve Eqns (4) in the stationary case when the incident radiation is focused, if its solution for a collimated beam is known. In particular, the formula for the self-focusing length L_{cr} (13) was modified for the case of a focused beam. In 2000 Milosevic et al. [103] considered in more detail the problem of a single pass through the MPC and showed that under two conditions, the B-integral << 1 and $(P/P_{cr})^2 \ll 1$, the Gaussian beam (TEM_{00} mode) is resistant to self-focusing. Namely, when propagating to the focal plane, part of the energy of the TEM_{00} mode is transferred to the TEM_{01} mode, but after the focal plane the direction of the energy flow changes, and as a result, all the energy from the TEM_{01} mode returns to the TEM_{00} mode. It is important to note the second degree in the last inequality, which allows one to 'approach' the critical power up to $P = 0.5P_{cr}$. This effect underlies the successful development of gas-MPCs, but until 2017 [169] it was ignored. Secondly, the transition from a solid-state nonlinear medium to a gas medium (as in the case of the transition from a silica fibre to capillaries) makes it possible to significantly increase P_{cr}, and, consequently, both P_{in} and P_{out}. Theoretical studies on the use of gas-MPCs can be found in [172–175], as well as in review [92] and references therein.

Thus, in MPCs, the power is limited by the P_{cr} value of the LSSF. In SS-MPCs, the nonlinear medium is thin and can be shorter than L_{cr}, which allows $P_{in} > P_{cr}$ (Section 3.3.1). In gas-MPCs (Section 3.3.2), P_{in} must be strictly less than P_{cr}, but the value of P_{in} itself is much larger due to the low value of n_2 in gases. The results of experiments with SS-MPCs [176–187] and gas-MPCs [125, 188–200] are presented in Figs 2–4 and described below.

3.3.1. Solid-state multipass cells (SS-MPCs). In the first experiment in 2016 [76], the nonlinear medium was located in a wide beam rather than at the focus. This geometry that was proposed in [165, 166]. Herriott cell mirrors were deposited onto the outer surfaces of fused silica substrates, which served as a nonlinear medium. In [176], the pulse was compressed by a factor of five and the output power P_{out} was 0.24 GW. In most subsequent works, nonlinear plates were located either in the waist or near it. It is important to note that the nonlinear medium in SS-MPCs is much shorter than that in fibres and capillaries, and this makes it possible to exceed the critical power P_{cr} if the length of the medium L is less than L_{cr}. This circumstance has been successfully exploited: for example, in [184], where (in the second compression stage) $P_{in} = 250$ MW, i.e., almost 100 times more than P_{cr} for fused silica. Substituting the parameters $L =$ 9.5 mm, $w = 0.22$ mm, and $B = 1.2$ (per pass) indicated in the work into formula (13), we obtain $L_{cr} = 2.1L$, which ensured the absence of catastrophic self-focusing. Song et al. [187] used values close to these in the second compression stage. Thus, although LSSF is the main effect limiting P_{in}, the threshold (in contrast to the fibre and capillary) is not P_{cr}, but a value about 100 times greater. On the other hand, in Refs [184, 187], L_{cr} is only slightly larger than L, and therefore further scaling is difficult. It is no coincidence that these works yielded record output power values for SS-MPCs: $P_{out} = 0.71$ and 0.68 GW, respectively.

The record value $F = 10.8$ was also obtained in [184], but in the first cascade. To date, SS-MPCs are characterised by relatively small F and long pulses: the minimum $T_{in} = 17$ fs was obtained after the second cascade in [186]. This makes the use of multistage compression relevant and popular. Thus, out of twelve experimental works [176–180, 182–187, 200], four [184–187] implemented two cascades, and one [179] utilised even three compression cascades.

Thus, SS-MPCs are close in power to SMF-PCFs, inferior to them in duration, and, accordingly, leave them behind in pulse energy. The pulse compression to several field cycles and a slight increase in the input power will lead to an increase in P_{out}, but it is unlikely that it will allow the level of tens of GW to be reached, which was obtained in the very first work with gas-MPCs.

3.3.2. Gas-filled multipass cells (gas-MPCs). The use of gas-MPCs was first demonstrated in 2018 almost simultaneously in two papers [188, 189], where P_{out} powers of 4.1 and 51 GW, respectively, were achieved. The same year, Kaumanns et al. [190] managed to obtain a subterawatt power (430 GW), and, finally, in 2021, the same group [195] reached $P_{out} = 2.9$ TW. Argon was used in all these works, and P_{in} was 25%–35% of P_{cr}, which increased from 2 GW [189] to 220 GW [195]. Such a significant increase in P_{cr} was

provided by a decrease in the argon pressure from 7 to 0.25 atm, as well as by using the Laguerre–Gauss vortex mode LG_{10} instead of the Gaussian beam, for which P_{cr} is four times larger than that for the Gaussian beam [201, 202]. The theory is described in detail in [175]. Note that in [190, 195], a very long input pulse (T_{in} = 1.3 ps) was used and a large compression factor was obtained ($F > 30$), which also ensured a large value of P_{out}. The cost of increasing P_{cr} and, accordingly, P_{in} is the increase in the waist diameter, which is necessary to avoid ionisation. This, in turn, inevitably leads to an elongation of the Herriott cell so that the intensity on the mirrors is less than the breakdown threshold. Thus, in the four experimental studies mentioned above, the cell lengths were 0.45 m [189], 1 m [188], 4 m [190], and 8 m [195].

The maximum compression factor F = 37 (the shortening of the pulse from 1200 to 32 fs) was obtained in [192], where the pulse was additionally compressed to 13 fs in the second stage, i.e., the total compression was almost two orders of magnitude. Work [196] is also noteworthy for several reasons. First, not two large-aperture mirrors were used, but several independently controlled mirrors, which made it possible to efficiently cool and align them. Secondly, P_{in} was close to P_{cr}, but the authors do not discuss this fact in any way. Third, the pulse duration T_{out} = 6.9 fs was obtained. The shortest pulse was obtained in [200]: T_{out} = 5.3 fs. Although the authors indicate that P_{in} was less than $0.5P_{cr}$ in this experiment, the value of P_{in} exceeded P_{cr} given by formula (12).

4. Free propagation of a laser beam

An alternative to waveguides is a bulk solid-state nonlinear element in which the laser beam propagates freely. The use of gases in this case is problematic due to their low nonlinearity and the impossibility of providing a large B-integral. For a solid-state nonlinear medium, the case of $P_{in} < P_{cr}$ is of little interest because of the small value of P_{cr}, and therefore the only possibility is to use thin nonlinear plates with lengths $L < L_{cr}$. To avoid breakdown at a high radiation power, the beam diameter must be large enough: for multiterawatt and petawatt power, from 1 to 10 cm or more. Thus, the geometry of the nonlinear medium changes radically – from a long cylinder to a thin disk. The increase in power, paradoxically, completely solves the problem of large-scale self-focusing. The point is that the focusing length L_{cr} at $P_{in} \gg P_{cr}$ decreases as $P_{in}^{-1/2}$, but grows as the square of the diameter, i.e., at a given intensity, L_{cr} increases (rather than decreases) in proportion to $P_{in}^{1/2}$ [see (13)]. In other words, the ratio L_{cr}/L grows in proportion to the beam radius w [see (14)], and for $w > 1$ mm, $L_{cr} \gg L$, i.e., LSSF can be neglected (here a solid nonlinear medium with a length of ~1 mm is implied). Note that for subpetawatt laser beams, $P_{in} \approx 10^8 P_{cr}$.

Free propagation has three drawbacks compared to waveguide propagation. First, cross-section inhomogeneous spectral broadening leads to inhomogeneous pulse compression: the compression factor F is proportional to the B-integral (11), which is proportional to the intensity. In particular, at the beam periphery, where the intensity is much lower than on the axis, the compression effect practically disappears. As a result, the value of F is less than that for the flat-top beam (11). This problem is pointed out in many papers [203–205] as the main limitation for SPM in the case of free beam propagation. For relatively small beam diameters, the nonlinear phase incursion can be made more uniform by resorting to noncollinear propagation, which is the subject of Section 4.1. For collinear propagation (see Section 4.2), this problem can be solved using a nonlinear element in the form of a negative lens, in which L varies over the beam cross section [206, 207]. In addition, the estimates given in [8] showed that, compared with a flat-top beam, for a super-Gaussian beam with exponent m, the compressed pulse power P_{out} at large B decreases by a factor of $2^{1/m}$, i.e., for m = 1 (Gaussian beam) P_{out} decreases two times, and for m = 4, only 1.08 times.

Second, the inhomogeneity of the spatial phase leads to nonlinear distortions of the wavefront. This degrades the focusability by reducing the focal intensity. Near the beam axis, the phase is proportional to r^2, and so it is convenient to divide the aberrations into two parts: parabolic and nonparabolic. The former are characterised by the focal length of a 'nonlinear lens' and, in fact, are not aberrations: it is enough to move the target closer to the focusing parabola. The diameter of the focal spot and the intensity of the focused radiation will not change in this case. Nonparabolic aberrations, on the other hand, are difficult to compensate for and result in reduced intensity at the focus. Qualitatively nonlinear beam aberrations were analysed by Hunt et al. [208]. If we neglect the dispersion, then the phase distribution is proportional to the B-integral. Thus, in the approximation of small aberrations, Perevezentsev et al. [209] obtained analytical formulae, which can be used to calculate the quantitative characteristics of aberrations – the parameter M^2 [210], the Strehl ratio [211], and the overlap integral. An analysis of these formulae showed [8] that the Strehl ratio S depends nonmonotonically on m. This is explained by the fact that as m increases, on the one hand, phase distortions 'are pressed' to the beam periphery, and on the other hand, the number of parabolic distortions decreases and the number of nonparabolic distortions increases significantly. To minimise aberrations, there is no need to strive for large values of m, because it is quite sufficient to have m = 2, and for $B < 6$ (less than 10), the Strehl ratio $S > 0.8$ (more than 0.7), i.e., aberrations will lead to a decrease in intensity at the focus by no more than 20% (30%). For a Gaussian beam and for a super-Gaussian beam with m = 5–8, the decrease in the focal intensity is more significant, especially at large B, which leads to a necessity of using an adaptive mirror. Adaptive mirrors are employed in many high-power lasers, in which case only a change in their software is required. Accounting for dispersion (both linear and nonlinear) greatly complicates the problem of nonlinear aberrations and their compensation, since the phase becomes a complex function of r and t – it cannot be represented as a product of functions of these parameters. A detailed numerical analysis of this problem is presented in [212]. Note that numerical simulations showed [31] that a super-Gaussian beam can be well focused at B = 48 and m = 8 even without an adaptive mirror.

Third, until recently it was assumed that effective compression during collimated propagation is impossible due to SSSF, which leads to an increase in the amplitude of spatial perturbations of a plane wave in a medium with cubic nonlinearity [38]. In contrast to large-scale self-focusing, SSSF is present even in a plane wave (in a flat-top beam). Due to SSSF, the beam is split into a large number (on the order of P_{in}/P_{cr}) of filaments, which significantly degrade the quality

of the beam and, ultimately, lead to the breakdown of optical elements. The instability increment is determined by the B-integral; it was argued that at $B > 2–3$ the beam inevitably splits into filaments. At $B = 3$, the power – even theoretically (11) – can increase only by a factor of 2.5. This argument, which is valid for nanosecond pulses, was erroneously transferred to femtosecond pulses (see, for example, Refs [165, 205, 213, 214]), and, unfortunately, continues to be repeated, including in recent reviews [16, 17]. Mironov et al. [215] demonstrated that high-power femtosecond lasers can effectively suppress SSSF by self-filtering the beam during propagation in free space, which served as a stimulus for experiments with collimated propagation. The issue of SSSF (for all geometries of a nonlinear element) and its suppression is considered in detail in Section 5.

The results of experiments with noncollinear free propagation (NCFP) of a focused beam [83, 151, 182, 186, 216–229] and with a collimated beam (TFC/CafCA) [230–246] are shown in Figs 2–4 and are described in Sections 4.1 and 4.2, respectively.

4.1. Noncollinear free propagation (NCFP)

The first work in which compression was implemented noncollinear free propagation of a focused beam (NCFP) was published in 1988 [229]. To increase spatial homogeneity, it was proposed to place a diaphragm immediately after the nonlinear element, thus leaving only the paraxial region of the beam. The authors experimentally investigated the trade-off between effective pulse shortening (minimum diaphragm size) and minimal energy loss (maximum diaphragm size). The results showed that quasi-homogeneous fourfold pulse compression is obtained when the diaphragm transmittance is no more than 25 %–35 %. Nevertheless, the output power P_{out} was 4 GW, three orders of magnitude higher than the record value at the time. In work [216], the beam was focused onto a nonlinear element by a cylindrical lens in such a way that soliton propagation was ensured in the smaller direction. However, the losses in this experiment were even greater. Mevel et al. [217] placed the diaphragm in the beam not immediately after the nonlinear element, but in the far field. This also led to a quasi-homogeneous compression of the pulse, with a diaphragm transmission being only 35 %. More than 50 % of the transmission was obtained with SPM in quartz after cleaning the beam in the filament in argon [218]. In this work, P_{out} = 30 GW; however, it is obvious that significant scaling of this idea is impossible.

Seidel et al. [219] studied in detail theoretically and experimentally the restrictions on the pulse power in the case of a nonlinear element located in the focal plane or near it. In the same work, an alternative approach was proposed: to use several non-linear elements. The thicknesses of the elements and the distances between them were chosen such that diffraction in free space was compensated for by self-focusing in nonlinear elements. Thus, it was possible to accumulate a significant B-integral. The theoretical substantiation of this idea is presented by Vlasov et al. [247], who showed that a periodic structure of linear and nonlinear media (with lengths L and l and refractive indices n_0 and 1, respectively) is a waveguide under the condition $\gamma P_{cr} < P_{in} < 2\gamma P_{cr}$, where $\gamma = n_0(L + l)/L$. Centurion et al [248] obtained numerically and experimentally similar results; see also [249]. In contrast to SS-MPCs, the waveguide properties here are provided exclusively by nonlinearity, and no mirrors are used. A more flexible approach allows for nonperiodicity: both the thicknesses of nonlinear elements and the distances between them can be different.

Lu et al. [250] used several nonlinear elements to generate the supercontinuum, and Cheng et al. [251] reported a detailed theoretical study. In the first experimental implementation of this approach, for the purpose of compression [220], the beam passed through seven nonlinear plates; a power P_{out} = 0.13 TW and a very high compression factor F = 5.6 were obtained. In subsequent papers [151, 182, 186, 221–226, 228], this approach was developed. In the second cascade, Lu et al. [223] demonstrated a record value F = 9.5 (pulse shortening from 30.6 to 3.21 fs). Note that, taking into account the first cascade, the pulse in this work was compressed from 170 to 3.21 fs. The shortest pulse, T_{out} = 2.6 fs, was obtained in [224], which is an absolute record for all compression geometries. We note work [227], in which compression was implemented in the UV range at a wavelength of 308 nm using SPM in a CaF_2 crystal.

The record power for NCFP was recently obtained by Stanfield et al. [226]: P_{out} = 0.15 TW (0.75 mJ, 7 fs), with the radiation intensity in the nonlinear element being 4 TW cm^{-2}. Moreover, in the same work, at the same intensity, but with a sevenfold increase in the input energy, a spectrum was recorded for which the duration of the Fourier-transform pulse was 8 fs. However, compression was not demonstrated due to the lack of chirped mirrors of the required aperture and optical damage threshold. Thus, the presently achieved parameters for noncollinear propagation are somewhat higher than those obtained using SS-MPCs, and in the near future they will reach the terawatt level in both gas-MPCs and SF-HCFs. It is possible to radically increase the power up to petawatts by using SPM with collinear propagation.

4.2. Collinear propagation (TFC/CafCA)

For collimated beams, as applied to super-high power lasers, the term TFC (thin film compression) [7] or CafCA (compression after compressor approach) [4, 8] is used. A collimated beam was first used as early as 1976 with SPM in liquid (CS_2) in [203], where the pulse was compressed from 96 to 6.9 ps. The idea of using of a collimated beam for compression of high-power femtosecond pulses at $B < 3$ was put forward by Mak and Yashin [213], who proposed to obtain large values of B by using several elements separated by spatial filters, which is difficult to implement in practice. Because of this, the idea was forgotten and rediscovered in patent [205] and analysed in detail in [166]. Vlasov et al. [165] showed that spatial filters can be abandoned, but the maximum value of B in one stage should be less than $\pi/2$, which also makes the idea impractical. Chvykov et al. [230] experimentally demonstrated the broadening of the spectrum at $B \approx 3$, after which the attenuated pulse was compressed from 30 to 14 fs. Several works are devoted to the numerical simulation of SPM of super-high power pulses [7, 31, 233]. A detailed study was carried out in [31], where the authors took into account not only all the effects described by Eqn (4), but also the ionisation nonlinearity, as well as the losses and dispersion introduced by the plasma formed during the ionisation of the medium by

the laser field. A Gaussian radiation pulse with a duration of 120 fs, a power of 13 PW, a beam diameter of 40 cm, and a super-Gaussian intensity distribution ($m = 8$, $I = 11$ TW cm^{-2}) was applied to the input of the nonlinear medium (fused silica). The simulation results showed that it is possible to compress the pulse to 25 fs with full dispersion compensation, and when using nine stages separated by eight spatial filters (which seems difficult to implement in practice), one can obtain a duration of 5.2 fs.

Ginzburg et al. [252] experimentally found that if the input pulse is not transform limited, then the nature of the broadened spectrum changes qualitatively: narrow peaks appear in the spectrum, and the broadening decreases. Detailed theoretical studies [8, 234, 252] showed that, despite this, such pulses can be compressed with almost the same compression factor as transform limited pulses.

As mentioned above, the inhomogeneity of the Gaussian beam leads to a twofold decrease in power compared to the flat-top beam. Lehmberg and McMahon [203] showed it numerically and the authors of [8] demonstrated it analytically. In order to 'return' this twofold decrease, Mironov et al. [206, 207] proposed to use a nonlinear element for SPM not in the form of a plane-parallel plate, but in the form of a negative lens. The lens parameters are chosen to minimise B-integral variations. The mirror then collimated the laser beam. This idea was implemented in works [231, 232] with a TF12 glass lens. In both papers, a compression factor $F > 2$, which is quasi-homogeneous over the beam cross section, was demonstrated. And in [232] P_{out} exceeded 10 TW, which is much larger than for all other compression geometries. It is important to note that in this work $B = 6$, but there was no SSSF as a result of using the method of beam self-filtering during propagation in free space proposed in [215] (see Section 5 for details).

In the following years, many experiments were carried out. In addition to silica, various polymeric nonlinear media have been studied [233, 234, 237, 243], which have a number of advantages: practically unlimited transverse size, thickness up to 100 μm or less, low cost, and the ability to use a roller mechanism [237], which makes it possible to roll a polymer film in the case of its degradation. Today, the main advantage – small thickness – is not so in demand, since the restrictions on the B-integral are removed (see Section 5), and so the results obtained with silica are more impressive: P_{out} = 250 TW, T_{out} = 14.5 fs (2018) [235]; P_{out} = 1 PW, T_{out} = 15.5 fs (2020) [240]; and P_{out} = 1.5 PW, T_{out} = 11 fs (2021) [244].

Shaykin et al. [245] proposed to use a KDP crystal instead of silica. The lower the ratio of the medium dispersion k_2 and nonlinear refractive index n_2, the shorter the compressed pulse [8]; and for KDP (ordinary wave) at a wavelength of 910 nm, the ratio k_2/n_2 is much smaller than for silica. Experiments [245] confirmed the promise of KDP: although slightly, the results were improved, and record values for TFP/CafCA were obtained: not only $P_{out} = 1.5$ PW and $F = 6$, but also T_{out} = 10 fs. The experiments were carried out [244, 245] with the B-integral from 5 to 19, and no damage was found to the optical elements, which indicates the suppression of small-scale self-focusing (see Section 5).

We also note the work by Kieffer et al. [246], who experimentally demonstrated that at $B \approx 3$, nonlinear aberrations reduce the Strehl ratio by only 10% even without the use of adaptive optics, which agrees with the theory [8].

5. Suppression of small-scale self-focusing in high-power laser beams

SSSF is a spatial instability of a plane wave propagating in a medium with cubic nonlinearity – an increase in the amplitude of spatial harmonic perturbations [38]. The first experimental observation [253] showed quantitative agreement with the theoretical predictions [38] and confirmed the qualitative difference between SSSF and LSSF. This theory was developed in the stationary approximation and experimentally confirmed in a large number of papers, including the fact that the instability increment is determined by the B-integral, the threshold value of which is approximately equal to 3. It has already been stated above that the argument that the beam at $B > 2–3$ inevitably splits into filaments, which is true for nanosecond pulses, is erroneous for femtosecond pulses. The consequence of this misconception is the opinion (see, for example, [16, 17, 165, 205, 213, 214]) about the impossibility of large compression factors that require large values of B (11), since the same parameter – B-integral – is both useful and harmful. Theoretical and experimental studies performed in the last few years show that this is not the case. In Section 5, we briefly discuss these results.

5.1. Beam self-filtering during free space propagation

Mironov et al. [215] proposed a method for suppressing SSSF, the idea of which is as follows (Fig. 5). If the optical element is located at a large distance from the noise source, then the most 'dangerous' noise components (with $\theta \sim \theta_{max}$) emerge from the beam aperture (outgoing beams are shown by dashes). The main sources of noise are the surfaces of mirrors or diffraction gratings; therefore, by placing an optical element at a sufficient distance L_f from the last mirror or grating, it is possible to remove 'dangerous' noise components from the region of interaction with a strong wave. For nanosecond lasers, the characteristic radiation intensity is a few GW cm^{-2}, which gives $\theta_{max} \sim 1$ mrad and makes self-filtering in free space practically impossible due to the too high value of L_f. For femtosecond lasers, the intensity is a few TW cm^{-2}, and the angle θ_{max} is much larger – tens of mrad, which leads to reasonable distances L_f. Thus, free space is a spatial filter, the transmission coefficient of

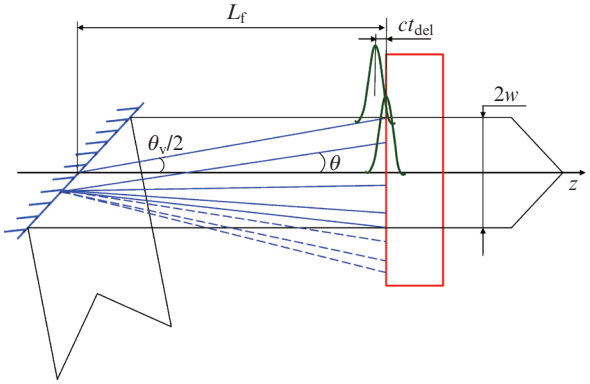

Figure 5. (Colour online) Noise filtering during free space propagation. Part of the spatial harmonics (dashed blue rays) do not fall into the beam aperture. The time lag is shown in green.

which for a flat-top beam is determined by the formula [8, 254]

$$T_{\text{space}}\left(\frac{\theta}{\theta_{\text{v}}}\right) = \frac{1}{\pi}\int_0^1 \arccos\left[\frac{(\theta/\theta_{\text{v}})^2 + y - 1}{2\sqrt{y}\,\theta/\theta_{\text{v}}}\right]\text{d}y, \qquad (16)$$

where $\theta_{\text{v}} = 2w/L_{\text{f}}$ is the viewing angle, and w is the beam radius.

Self-filtering of intense radiation was confirmed in Refs [215, 255] using qualitative experiments. In [215], when the frequency was doubled in a KDP crystal at $B = 6$, filamentation and breakdown of the crystal were observed at a viewing angle $\theta_{\text{v}} = 40$ mrad and were completely absent at $\theta_{\text{v}} = 10$ mrad. Mironov et al. [255] measured the degradation of a 4-mm-thick glass plate after irradiation with 100 single-point pulses, and the results clearly confirmed the self-filtering effect at small viewing angles θ_{v}. Ginzburg et al. [256] confirmed the effect quantitatively: the spatial spectrum of the noise amplification factor was measured as a function of L_{f}. The measurements were performed by two independent methods: direct [42, 257] and indirect [257]. The beam passed through a thin (0.2 mm) slightly frosted glass plate introducing noise. A glass plate 10 mm thick served as a nonlinear element. Both the direct and indirect methods gave good agreement with the theory. Note that, for narrow beams, self-filtering occurs at very small L_{f} (on the order of 50 mm at $w = 1$ mm and 0.5 mm at $w = 10$ μm), as if by itself as one can say, as was first pointed out by Lehmberg and McMahon [203]. This is the reason for the absence of SSSF with SPM in fibres and capillaries.

For short pulses, free space is also a temporal filter separating noise radiation from the main one not in space, but in time. Since noise radiation propagates at an angle to the z axis, it lags behind the main pulse. If the delay time t_{del} is commensurate with the pulse duration T_{in}, then its maximum will 'meet' the leading edge of the noise, which is equivalent to noise reduction (Fig. 5). Assuming that the pulse has a Gaussian shape, it is easy to obtain the transmission of such a filter

$$T_{\text{time}} = \exp\left[-\ln 2\left(\frac{L_{\text{f}}}{\lambda}\frac{\theta^2}{N}\right)^2\right]; \qquad (17)$$

T_{time} is independ of the beam aperture, but depends on the duration, while T_{space} does the opposite. Note the very sharp dependence of T_{time} on the angle θ in (17).

5.2. Noise spectral density reduction at large angles

Another positive consequence of the large value of $\theta_{\max}$ is the fact that the noise spectral density obviously decreases with increasing θ. The shapes of the spectrum, as well as the spectral noise densities for amplitude and phase noise, differ. The amplitude noise is caused by optical defects leading to zero intensity at some points of the beam cross section: dust particles and scratches. The reason for phase noise is the distortion of the wavefront introduced by the optical elements. The inhomogeneity of the refractive index is usually large-scale and does not contribute much to the noise at high spatial frequencies, while the surface profile of optical elements, on the contrary, contains the entire spectrum. The spectral noise density is determined by the spectral density of the surface profile. Ginzburg et al. [254] performed calculations for model spectra of amplitude and phase noise. The results showed that this effect can significantly reduce SSSF; however, the quantitative results strongly depend on the law of spectral density reduction, which requires an experimental study.

5.3. Increasing the critical angle of SSSF

As shown above, an increase in $\theta_{\max}$ makes it possible to suppress the development of SSSF. In other words, it is advantageous to increase $\theta_{\max}$, which, according to (15), can be done by increasing intensity or media with larger n_2. Many crystals (KDP, YAG, TGG, and BBO) have two to three times higher n_2 than fused silica. It may be promising to use a paratellurite crystal, in which n_2 is 21 times greater than that of fused silica [258]. However, this will require the manufacture of very thin samples, which is not so simple. Polymer media are free of this shortcoming; their thickness can be 100 μm or less. The value of n_2 in some polymers is two to three times greater than that of fused silica [243, 259], but given the wide variety of polymers, materials with even higher n_2 can be expected.

The authors of Ref. [8] drew attention to the fact that the installation of a nonlinear element at a grazing angle of incidence is equivalent to an increase in $\theta_{\max}$, since the ratio between the internal and external angles changes. In particular, if the angle of incidence is equal to the Brewster angle, the effective value of $\theta_{\max}$ will be equal to $n_0\theta_{\max}$. At even larger angles of incidence, the gain will be even greater. We note that usually media with a large n_2 also have a large n_0, and to increase $\theta_{\max}$ it is advantageous to increase both refractive indices, with $\theta_{\max}$ being proportional to $n_2^{1/2}n_0^{3/2}$ at the Brewster angle of incidence. For example, for a TGG crystal, the gain compared to silica will be almost four times.

5.4. Fragmentation of a nonlinear element

Fragmentation of a nonlinear element is the replacement of one element with M elements with the same total length L without repeaters or spatial filters between them. For large values of $\theta_{\max}$ – tens of mrad – the noise phase incursion in free space reaches 2π at distances L_{f} of about 1 mm. Therefore, at distances between nonlinear elements of 1 cm or longer, the noise phase at the input to each nonlinear element can be considered random. In this case, the total gain in M nonlinear elements will be equal to the product of the gains in each, which is less by approximately 2^{M-1} times than for one element of length L [8]. Even greater SSSF suppression can be achieved by using nonlinear elements with significantly different n_2 or I (in the latter case, a convergent or divergent beam should be used). Noise gain maxima in two (or more) nonlinear elements will be reached at significantly different values of θ, due to which the product of the gains will be less than for one element of length L.

Note that fragmentation makes it possible to suppress SSSF due to phase effects as well. By changing the distances between the elements, it is possible to change the noise phase at the input to the second nonlinear element, thereby controlling the noise gain [39]. In optical systems consisting of a periodic sequence of linear and nonlinear media, it is possible to suppress SSSF not for all, but for many angles θ [40, 260, 261]. It is more efficient to use non-equidistant geometry, in which the thicknesses of nonlinear elements and the distances between them are different, which was observed experimentally [262, 263] and was explained theoretically [262, 264]. In all these works, SSSF of nanosecond pulses was studied.

5.5. SSSF suppression due to nonlinear dispersion

Balakin et al. [33, 34] studied the development of SSSF for laser pulses with a small number of field oscillations. They showed analytically that the homogeneous solution remains unstable, but the type of instability changes, i.e. it becomes convective. They also demonstrated numerically that for laser pulses with a duration shorter than a certain value, SSSF does not develop. Physically, this is explained by the fact that the intensity perturbations, having a lower group velocity, lag behind and shift to the trailing edge of the pulse, where the intensity is much lower and their growth slows down. An estimate of the pulse duration at which the growing perturbations are stabilised as a result of their shift to the trailing edge of the pulse gave a value on the order of ten cycles of the laser field oscillations. Thus, for short pulses, a SSSF suppression mechanism is predicted that does not require any special efforts and devices. Experimental confirmation of the effect of SSSF suppression due to nonlinear dispersion has not yet been demonstrated.

6. Conclusions

Table 1 summarises the most important aspects of the compression of femtosecond laser pulses using self-phase modulation for eight variants of the nonlinear medium geometry. Figure 2 shows that currently the most dynamically developing variants for using SF-HCF, gas-MPC and TFC/CafCA. It is in these variants of geometry that further progress should be expected in the coming years. One can see from Table 1 and Figs 2–4 that, in applications to super-high power lasers, the use of TFC/CafCA is the only option for pulse compression. It is also important to note that although this is the cheapest and simplest technology (see Fig. 1), it has virtually no power limit. Let us briefly list the most relevant areas for further research on TFC/CafCA technology.

1. Despite a number of studies, including experimental confirmation of SSSF suppression up to $B = 19$ [244, 245], there is still no complete understanding of all the mechanisms of this suppression (see Section 5).

2. The optical damage threshold of nonlinear elements, in which the emission spectrum is broadened, is greater than that of compressor diffraction gratings, and therefore it is not a power limitation, but the optical damage threshold of chirped mirrors may become such a limitation in the future. In this regard, it is of interest to develop the technology of wide-aperture chirped mirrors with a high breakdown threshold, as well as alternative dispersive elements [265].

3. The study of the beam focusing quality, including with the help of an adaptive mirror, has practically only begun (see Section 4) and, despite encouraging results [8, 31, 212, 246], requires further theoretical and experimental studies.

4. As can be seen from Figs 3, 4, the range of pulse durations mastered with the help of TFC/CafCA is relatively nar-

Table 1. Comparison of different SPM geometries.

	Continuous waveguide				Discrete waveguide		Free propagation	
	Fibre (SMF)		Capillary (HCF)		Herriott multipass cell (MPC)			
	SMF-TIR	SMF-PCF	TW-HCF	SF-HCF	SS-MPC	gas-MPC	NCFP	TFC/CafCA
Power increase limitations								
SSSF	yes	no	yes	yes	yes	no	yes	no
LSSF	no	no	no	no	no	no	yes	yes
Optical breakdown	yes	yes	yes	yes	yes	no	yes	no
Inhomogeneity	no	no	no	no	no	no	yes	yes
Typical parameters								
Nonlinear medium	solid	solid/gas	gas	gas	solid	gas	solid	solid
Critical power P_{cr}	3 MW	–	30 GW	30 GW	3 MW	30 GW	3 MW	3 MW
Breakdown threshold P_{br}	10 MW	100 MW	100 GW	100 GW	10 GW	100 GW	100 GW	>10 PW
Input power P_{in}	1 MW	30 MW	30 GW	30 GW	100 MW	10 GW	30 GW	TW – PW
Input energy	1 μJ	30 μJ	3 μJ	3 μJ	10 μJ	10 mJ	0.3 mJ	0.1 – 10 J
Beam radius w/mm	0.01	0.03	0.3	0.5	1	0.5	1	30
Number of modes	one	many	many	many	one	one	one	one
Records								
Output power P_{out}	100 MW [64]	1.5 GW [58]	1.2 TW [127]	1.6 TW [155]	0.7 GW [184, 187]	2.9 TW [195]	0.13 TW [220, 223]	1.5 PW [244, 245]
Output duration T_{out}/fs	4.6 [60]	4.4 [76]	3.4 [120]	3.4 [154]	17 [186]	5.3 [200]	2.6 [224]	10 [245]
Compression factor $F = T_{in}/T_{out}$	80 [94]	24 [84]	18 [144]	48 [156]	10.8 [187]	37.5 [192]	9.6 [223]	6 [245]
Papers								
Idea	[90]	[84]	[98, 99]	[107]	[165, 166]	[169]	[229]	[203, 213]
First experiment	[49]	[84]	[98, 99]	[147]	[176]	[188, 189]	[229]	[230]
All experiments	[49 – 69]	[70 – 89]	[98, 100, 106, 108 – 146]	[147 – 159]	[176 – 187]	[125, 188 – 200]	[83, 151, 182, 186, 216 – 229]	[230 – 246]
Reviews	–	[48]	[6, 16]	[16]	[17]	[17]		[8]

row: the maximum T_{in} = 126 fs, and the minimum T_{out} = 10 fs. Extremely promising is both advancement to durations of one field cycle, which opens up a new way for petawatt lasers, and compression of picosecond pulses, which will make it possible to significantly increase both the compression factor F and the output power P_{out}.

5. Search for new non-linear media (polymer, glass, crystalline) is needed, which will improve the compression parameters, for example, due to a large ratio of the nonlinear refractive index n_2 to the dispersion k_2.

Acknowledgements. The work was supported by the Ministry of Science and Higher Education of the Russian Federation (State Assignment No. 0030-2021-0015).

References

1. Maiman T. *Nature*, **187**, 493 (1960).
2. Brabec T., Krausz F. *Rev. Mod. Phys*., **72**, 545 (2000).
3. Krausz F., Ivanov M. *Rev. Mod. Phys*., **81**, 163 (2009).
4. Danson C., Bromage J., Butcher T., Chanteloup J.-C., Chowdhury E., Galvanauskas A., Gizzi L., Haefner C., Hein J., Hillier D., Hopps T., Kato Y., Khazanov E., Kodama R., Korn G., Li R., Li Y., Limpert J., Ma J., Nam C.H., Neely D., Papadopoulos D., Penman R., Qian L., Rocca J., Shaykin A., Siders C., Spindloe C., Szatmári S., Trines R., Zhu J., Zhu P., Zuegel J. *High Power Laser Sci. Eng*., **7**, e54 (2019).
5. Strickland D., Mourou G. *Opt. Commun*., **56**, 219 (1985).
6. De Silvestri S., Nisoli M., Sansone G., Stagira S., Svelto O. *Top. Appl. Phys*., **95**, 137 (2004).
7. Mourou G., Mironov S., Khazanov E., Sergeev A. *Europ. Phys. J.–Spec. Top*., **223**, 1181 (2014).
8. Khazanov E.A., Mironov S.Yu., Mourou G. *Phys. Usp*., **62**, 1096 (2019) [*Usp. Fiz. Nauk*., **189**, 1173 (2019)].
9. Giordmaine J.A., Duguay M.A., Hansen J.W. *IEEE J. Quantum Electron*., **QE-4**, 252 (1968).
10. Klauder J.R. *Bell Syst. Tech. J*., **39**, 809 (1960).
11. Klauder J.R., Price A.C., Darlington S., Albersheim W.J. *Bell Syst. Tech. J*., **39**, 745 (1960).
12. Duguay M.A., Hansen J.W. *Appl. Phys. Lett*., **14**, 14 (1969).
13. Gires F., Tournois P.C.R. *Acad. Sc. Paris*, **258**, 6112 (1964).
14. Fisher R.A., Kelley P.L., Gustajson T.K. *Appl. Phys. Lett*., **14**, 140 (1969).
15. Laubereau A. *Phys. Lett*., **29A**, 539 (1969).
16. Nagy T., Simon P., Veisz L. *Adv. Phys. X*, 6, 1845795 (2020).
17. Hanna M., Guichard F., Daher N., Bournet Q., Delen X., Georges P. *Laser Photonics Rev*., **15** (12), 2100220 (2021).
18. Kandidov V.P., Golubtsov I.S., Kosareva O.G. *Quantum Electron*., **34**, 348 (2004) [*Kvantovaya Elektron*., **34**, 348 (2004)].
19. Bergé L., Skupin S., Nuter R., Kasparian J., Wolf J.-P. *Rep. Prog. Phys*., **70**, 1633 (2007).
20. Berge L., Mauger S., Skupin S. *Phys. Rev. A*, **81**, 013817 (2010).
21. Ranka J.K., Gaeta A.L. *Opt. Lett*., **23**, 534 (1998).
22. Ostrovsky L.A. *Sov. Phys. Tech. Phys*., **8**, 679 (1965) [*Zh. Tekh. Fiz*., **33**, 905 (1963)].
23. Gustafson T.K., Tarant J.P., Haus H.A., Lifsitz J.R., Kelley P.L. *Phys. Rev*., **177**, 306 (1969).
24. DeMartini F., Nownes C.H., Gustafson T.K., Kelley P.L. *Phys. Rev*., **164**, 312 (1967).
25. Anderson D.P., Lisak M. *Phys. Rev. A*, **27**, 1393 (1983).
26. Shumakova V., Malevich P., Ališauskas S., Voronin A., Zheltikov A.M., Faccio D., Kartashov D., Baltuška A., Pugžlys A. *Nat. Commun*., **7**, 12877 (2016).
27. Voronin A.A., Zheltikov A.M. *Phys. Rev. A*, **94**, 023824 (2016).
28. Hemmer M., Baudisch M., Thai A., Couairon A., Biegert V. *Opt. Express*, **21**, 28095 (2013).
29. Voronin A.A., Zheltikov A.M. *Phys. Usp.*, **59**, 869 [2016) [*Usp. Fiz. Nauk*, **186**, 957 (2016)].
30. Schmidt B.E., Béjot P., Giguère M., Shiner A.D., Trallero-Herrero C., Bisson É., Kasparian J., Wolf J.-P., Villeneuve D.M., Kieffer J.-C., Corkum P.B., Légaré F. *Appl. Phys. Lett*., **96**, 121109 (2010).
31. Voronin A.A., Zheltikov A.M., Ditmire T., Rus B., Korn G. *Opt. Commun*., **291**, 299 (2013).
32. Kalosha V.P., Herrmann J. *Phys. Rev. A*, **62**, 011804(R) (2000).
33. Balakin A.A., Litvak A.G., Mironov V.A., Skobelev S.A. *J. Opt.*, **19**, 095503 (2017).
34. Balakin A.A., Kim A.V., Litvak A.G., Mironov V.A., Skobelev S.A. *Phys. Rev*., **94**, 043812 (2016).
35. Goldberg V.N., Talanov V.I., Erm R.E. *Radiophys. Quantum Electron*., **10**, 368 (1967) [*Izv. Vyssh. Uchebn. Zaved., Ser. Radiofiz*., **10**, 674 (1967)].
36. Marburger J.H. *Prog. Quantum Electron*., **4**, 35 (1975).
37. Kelley P.L. *Phys. Rev. Lett*., **15**, 1005 (1965).
38. Bespalov V.I., Talanov V.I. *Pis'ma Zh. Esp. Teor. Fiz*., **3**, 471 (1966).
39. Rozanov N.N., Smirnov V.A. *Sov. J. Quantum Electron*., **7**, 232 (1980) [*Kvantovaya Electron*., **7**, 410 (1980)].
40. Rozanov N.N., Smirnov V.A. *Sov. Phys. Tech. Phys. Lett*., **5**, 222 (1979) [*Pis'ma Zh. Tekh. Fiz*., **5**, 544 (1979)].
41. Garanin S.G., Epatko I.V., Lvov L.V., Serov R.V., Sukharev S.A. *Quantum Electron*., **37**, 1159 (2007) [*Kvantovaya Elektron*., **37**, 1159 (2007)].
42. Poteomkin A.K., Martyanov M.A., Kochetkova M.S., Khazanov E.A. *IEEE J. Quantum Electron*., **45**, 336 (2009).
43. Couairon A., Mysyrowicz A. *Phys. Rep*., **441**, 47 (2007).
44. Knight J.C., Birks T.A., Russell P.S.J., Atkin D.M. *Opt. Lett*., **21**, 1547 (1996).
45. Cregan R.F., Mangan B.J., Knight J.C., Birks T.A., Russell P.S., Roberts P.J., Allan D.C. *Science*, **285**, 1537 (1999).
46. Debord B., Amsanpally A., Alharbi M., Vincetti L., Blondy J.-M., Gérôme F., Benabid F. *J. Lightwave Technol*., **33**, 3630 (2015).
47. Stutzki F., Jansen F., Otto H.-J., Jauregui C., Limpert J., Tünnermann A. *Optica*, **1**, 233 (2014).
48. Markos C., Travers J.C., Abdolvand A., Eggleton B.J., Bang O. *Rev. Mod. Phys*., **89**, 045003 (2017).
49. Nakatsuka H., Grischkowsky D., Balant A.C. *Phys. Rev. Lett*., **47**, 910 (1981).
50. Shank C.V., Fork R.L., Yen R., Stolen R.H., Tomlinson W.J. *Appl. Phys. Lett*., **40**, 761 (1982).
51. Nikolaus B., Grischkowsky D. *Appl. Phys. Lett*., **42**, 1 (1983).
52. Nikolaus B., Grischkowsky D. *Appl. Phys. Lett*., **43**, 228 (1983).
53. Halbout J.-M., Grischkowsky D. *Appl. Phys. Lett*., **45**, 1281 (1984).
54. Fujimoto J.G., Weiner A.M., Ippen E.P. *Appl. Phys. Lett*., **44**, 832 (1984).
55. Damm T., Kaschke M., Noack F., Wilhelmi B. *Opt. Lett*., **10**, 176 (1985).
56. Knox W.H., Fork R.L., Downer M.C., Stolen R.H., Shank C.V., Valdmanis J.A. *Appl. Phys. Lett*., **46**, 1120 (1985).
57. Zysset B., Hodel W., Beaud P., Weber H.P. *Opt. Lett*., **11**, 156 (1986).
58. Fork R.L., Brito Cruz C.H., Becker P.C., Shank C.V. *Opt. Lett*., **12**, 483 (1987).
59. Sarukura N., Ishida Y., Nakano H. *Opt. Lett*., **16**, 153 (1991).
60. Baltuška A., Wei Z., Pshenichnikov M.S., Wiersma D.A., Szipocs R. *Appl. Phys. B*, **65**, 175 (1997).
61. Baltuska A., Wei Z., Pshenichnikov M.S., Wiersma D.A. *Opt. Lett*., **22**, 102 (1997).
62. Saraceno C.J., Heckl O.H., Baer C.R.E., Südmeyer T., Keller U. *Opt. Express*, **19**, 1395 (2011).
63. Lefort C., Mansuryan T., Louradour F., Barthelemy A. *Opt. Lett*., **36**, 292 (2011).
64. Guichard F., Zaouter Y., Hanna M., Morin F., Honninger C., Mottay E., Druon F., Georges P. *Opt. Lett*., **38**, 4437 (2013).
65. Pupeza I., Holzberger S., Eidam T., Carstens H., Esser D., Weitenberg J., Rußbüldt P., Rauschenberger J., Limpert J., Udem T., Tünnermann A., Hänsch T.W., Apolonski A., Krausz F., Fill E. *Nat. Photonics*, **7**, 608 (2013).
66. Klenke A., Hadrich S., Kienel M., Eidam T., Limpert J., Tunnerman A. *Opt. Lett*., **39**, 3520 (2014).
67. Liu W., Schimpf D.N., Eidam T., Limpert J., Tünnermann A., Kärtner F.X., Chang G. *Opt. Lett*., **40**, 151 (2015).
68. Carstens H., Högner M., Saule T., Holzberger S., Lilienfein N., Guggenmos A., Jocher C., Eidam T., Esser D., Tosa V., Pervak V., Limpert J., Tünnermann A., Kleineberg U., Krausz F., Pupeza I. *Optica*, **3**, 366 (2016).

69. Klenke A., Kienel M., Eidam T., Hädrich S., Limpert J., Tünnermann A. *Opt. Lett*., **38**, 4593 (2013).
70. Emaury F., Saraceno C.J., Debord B., Ghosh D., Diebold A., Gèrôme F., Südmeyer T., Benabid F., Keller U. *Opt. Lett*., **39**, 6843 (2014).
71. Köttig F., Tani F., Biersach C.M., Travers J.C., Russell P.S.J. *Optica*, **4**, 1272 (2017).
72. Mak K.F., Seidel M., Pronin O., Frosz M.H., Abdolvand A., Pervak V., Apolonski A., Krausz F., Travers J.C., Russell P.S.J. *Opt. Lett*., **40**, 1238 (2015).
73. Hädrich S., Krebs M., Hoffmann A., Klenke A., Rothhardt J., Limpert J., Tünnermann A. *Light Sci. Appl*., **4**, e320 (2015).
74. Guichard F., Giree A., Zaouter Y., Hanna M., Machinet G., Debord B., Gèrôme F., Dupriez P., Druon F., Hönninger C., Mottay E., Benabid F., Georges P. *Opt. Express*, **23**, 7416 (2015).
75. Köttig F., Schade D., Koehler J.R., Russell P.S.J., Tani F. *Opt. Express*, **28**, 9099 (2020).
76. Ermolov A., Heide C., Dienstbier P., Köttig F., Tani F., Hommelhoff P., Russell P.S.J. *Opt. Lett*., **44**, 5005 (2019).
77. Jocher C., Eidam T., Hädrich S., Limpert J., Tünnermann A. *Opt. Lett*., **37**, 4407 (2012).
78. Emaury F., Diebold A., Saraceno C.J., Keller U. *Optica*, **2**, 980 (2015).
79. Saule T., Holzberger S., De Vries O., Plötner M., Limpert J., Tünnermann A., Pupeza I. *Appl. Phys. B*, **123**, 17 (2017).
80. Vernaleken Andreas, Weitenberg Johannes, Sartorius Thomas, Russbueldt Peter, Schneider Waldemar, Stebbings Sarah L., Kling Matthias F., Hommelhoff Peter, Hoffmann Hans-Dieter, Poprawe Reinhart, Krausz Ferenc, Hänsch Theodor W., Udem T. *Opt. Lett*., **36**, 3428 (2011).
81. Niu F., Li J., Yang W., Zhang Z., Wang A. *IEEE Photonics Technol. Lett*., **30**, 1479 (2018).
82. Emaury F., Dutin C.F., Saraceno C.J., Trant M., Heckl O.H., Wang Y.Y., Schriber C., Gerome F., Südmeyer T., Benabid F., Keller U. *Opt. Express*, **21**, 4986 (2013).
83. Pronin O., Seidel M., Lücking F., Brons J., Fedulova E., Trubetskov M., Pervak V., Apolonski A., Udem T., Krausz F. *Nat. Commun*., **6**, 6988 (2015).
84. Südmeyer T., Brunner F., Innerhofer E., Paschotta R., Furusawa K., Baggett J.C., Monro T.M., Richardson D.J., Keller U. *Opt. Lett*., **28**, 1951 (2003).
85. Mak K.F., Travers J.C., Joly N.Y., Abdolvand A., Russell P.S.J. *Opt. Lett*., **38**, 3592 (2013).
86. Gebhardt M., Gaida C., Hädrich S., Stutzki F., Jauregui C., Limpert J., Tünnermann A. *Opt. Lett*., **40**, 2770 (2015).
87. Murari K., Stein G.J., Cankaya H., Debord B., Gèrôme F., Cirmi G., Mücke O.D., Li P., Ruehl A., Hartl I., Hong K.-H., Benabid F., Kärtner F.X. *Optica*, **3**, 816 (2016).
88. Liu W., Li C., Zhang Z., Kärtner F.X., Chang G. *Opt. Express*, **24**, 15328 (2016).
89. Heckl O.H., Saraceno C.J., Baer C.R.E., Südmeyer T., Wang Y.Y., Cheng Y., Benabid F., Keller U. *Opt. Express*, **19**, 19142 (2011).
90. Stolen R.H., Lin C. *Phys. Rev. A*, **17**, 1448 (1978).
91. Grischkowsky D., Balant A.C. *Appl. Phys. Lett*., **41**, 1 (1982).
92. Tomlinson W.J., Stolen R.H., Shank C.V. *J. Opt. Soc.Am. B*, **1**, 139 (1984).
93. Meinel R. *Opt. Commun*., **47**, 343 (1983).
94. Johnson A.M., Stolen R.H., Simpson W.M. *Appl. Phys. Lett*., **44**, 729 (1984).
95. Balakin A.A., Skobelev S.A., Andrianov A.V., Anashkina E.A., Litvak A.G. *Opt. Lett*., **46**, 246 (2021).
96. Andrianov A.V., Kalinin N.A., Anashkina E.A. *Laser Phys. Lett*., **18**, 125104 (2021).
97. Konorov S.O., Sidorov-Biryukov D.A., Zheltikova A.M. *Appl. Phys. Lett*., **85**, 3690 (2004).
98. Nisoli M., Silvestri S.D., Svelto O. *Appl. Phys. Lett*., **68**, 2793 (1996).
99. Ippen E.P., Shank C.V., Gustafson T.K. *Appl. Phys. Lett*., **24**, 190 (1974).
100. Zhou J.Y., Wang H.Z., Huang X.G., Cai Z.G., Yu Z.X. *Opt. Lett*., **16**, 1865 (1991).
101. Vozzi M.N.C., Sansone G., Stagira S., de Silvestri S. *Appl. Phys. B*, **80**, 285 (2005).
102. Tempea G., Brabec T. *Opt. Lett*., **23**, 762 (1998).
103. Milosevic N., Tempea G., Brabec T. *Opt. Lett*., **25**, 672 (2000).
104. Fibich G., Gaeta A.L. *Opt. Lett*., **25**, 335 (2000).
105. Tempea G., Brabec T. *Opt. Lett*., **23**, 1286 (1998).
106. Stagira S., Priori E., Sansone G., Nisoli M., De Silvestri S., Gadermaier C. *Phys. Rev. A*, **66**, 033810 (2002).
107. Nagy T., Forster M., Simon P. *Appl. Opt*., **47**, 3264 (2008).
108. Sartania S., Cheng Z., Lenzner M., Tempea G., Spielmann C., Krausz F., Ferencz K. *Opt. Lett*., **22**, 1562 (1997).
109. Nisoli M., Silvestri S.D., Svelto O., Szipöcs R., Ferencz K., Spielmann C., Sartania S., Krausz F. *Opt. Lett*., **22**, 522 (1997).
110. Nisoli M., Stagira S., De Silvestri S., Svelto O., Sartania S., Cheng Z., Lenzner M., Spielmann C., Krausz F. *Appl. Phys. B*, **65**, 189 (1997).
111. Nisoli M., Stagira S., De Silvestri S., Svelto O., Sartania S., Cheng Z., Tempea G., Spielmann C., Krausz F. *IEEE J. Sel. Top. Quantum Electron*., **4**, 414 (1998).
112. Cerullo G., De Silvestri S., Nisoli M., Sartania S., Stagira S., Svelto O. *IEEE J. Sel. Top. Quantum Electron*., **6**, 948 (2000).
113. Nisoli M., Sansone G., Stagira S., Vozzi C., De Silvestri S., Svelto O. *Appl. Phys. B*, **75**, 601 (2002).
114. Schenkel B., Biegert J., Keller U., Vozzi C., Nisoli M., Sansone G., Stagira S., De Silvestri S., Svelto O. *Opt. Lett*., **28**, 1987 (2003).
115. Suda A., Hatayama M., Nagasaka K., Midorikawa K. *Appl. Phys. Lett*., **86**, 111116 (2005).
116. Oishi Y., Sudaa A., Midorikawa K., Kannari F. *Rev. Sci. Instrum*., **76**, 093114 (2005).
117. Sung J.H., Park J.Y., Imran T., Lee Y.S., Nam C.H. *Appl. Phys. B*, **82**, 5 (2006).
118. Robinson J.S., Haworth C.A., Teng H., Smith R.A., Marangos J.P., Tisch J.W.G. *Appl. Phys. B*, **85**, 525 (2006).
119. Mansour B.F., Anis H., Zeidler D., Corkum P.B., Villeneuve D.M. *Opt. Lett*., **31**, 3185 (2006).
120. Cavalieri A.L., Goulielmakis E., Horvath B., Helml W., Schultze M., Fieß M., Pervak V., Veisz L., Yakovlev V.S., Uiberacker M., Apolonski A., Krausz F., Kienberger R. *New J. Phys*., **9**, 242 (2007).
121. Bohman S., Suda A., Kaku M., Nurhuda M., Kanai T., Yamaguchi S., Midorikawa K. *Opt. Express*, **16**, 10684 (2008).
122. Chen J., Suda A., Takahashi E., Nurhuda M., Midorikawa K. *Opt. Lett*., **33**, 2992 (2008).
123. Akturk S., Arnold C.L., Zhou B., Mysyrowicz A. *Opt. Lett.*, **34**, 1462 (2009).
124. Park J., Lee J.-h., Nam C.H. *Opt. Lett*., **34**, 2342 (2009).
125. Lavenu L., Natile M., Guichard F., Délen X., Hanna M., Zaouter Y., Georges P. *Opt. Express*, **27**, 1958 (2019).
126. Hädrich S., Rothhardt J., Eidam T., Limpert J., Tünnermann A. *Opt. Express*, **17**, 3913 (2009).
127. Fourcade Dutin C., Dubrouil A., Petit S., Mével E., Constant E., Descamps D. *Opt. Lett*., **35**, 253 (2010).
128. Arnold C.L., Zhou B., Akturk S., Chen S., Couairon A. Mysyrowicz A. *New J. Phys*., **12**, 073015 (2010).
129. Bohman S., Suda A., Kanai T., Yamaguchi S., Midorikawa K. *Opt. Lett*., **35**, 1887 (2010).
130. Anderson A., Lücking F., Prikoszovits T., Hofer M., Cheng Z., Neacsu C.C., Scharrer M., Rammler S., Russell P.S.J., Tempea G., Assion A. *Appl. Phys. B*, **103**, 531 (2011).
131. Andriukaitis G., Kartashov D., Lorenc D., Pugžlys A., Baltuška A., Giniūnas L., Danielius R., Limpert J., Clausnitzer T., Kley E.-B., Voronin A., Zheltikov A.M. *Opt. Lett*., **36** (10), 1914 (2011).
132. Rothhardt J., Hädrich S., Carstens H., Herrick N., Demmler S., Limpert J., Tünnermann A. *Opt. Lett*., **36**, 4605 (2011).
133. Auguste T., Gobert O., Dutin C.F., Dubrouil A., Mével E., Petit S., Constant E., Descamps D. *J. Opt. Soc. Am. B*, **29**, 1277 (2012).
134. Schweinberger W., Sommer A., Bothschafter E., Li J., Krausz F., Kienberger R., Schultze M. *Opt. Lett*., **37**, 3573 (2012).
135. Okell W.A., Witting T., Fabris D., Austin D., Bocoum M., Frank F., Ricci A., Jullien A., Walke D., Marangos J.P., Lopez-Martens R., Tisch J.W.G. *Opt. Lett*., **38**, 3918 (2013).
136. Hädrich S., Klenke A., Hoffmann A., Eidam T., Gottschall T., Rothhardt J., Limpert J., Tünnermann A. *Opt. Lett*., **38** (19), 3866 (2013).
137. Jarnac A., Brizuela F., Heyl C.M., Rudawski P., Campi F., Kim B., Rading L., Johnsson P., Mysyrowicz A., L'Huillier A., Houard A., Arnold C.L. *Eur. Phys. J. D*, **68**, 373 (2014).
138. Lücking F., Trabattoni A., Anumula S., Sansone G., Calegari F., Nisoli M., Oksenhendler T., Tempea G. *Opt. Lett*., **39** (8), 2302 (2014).

139. Rothhardt J., Hädrich S., Klenke A., Demmler S., Hoffmann A., Gotschall T., Eidam T., Krebs M., Limpert J., Tünnermann A. *Opt. Lett*., **39**, 5224 (2014).
140. Hädrich S., Klenke A., Rothhardt J., Krebs M., Hoffmann A., Pronin O., Pervak V., Limpert J., Tünnermann A. *Nat. Photonics*, **8**, 779 (2014).
141. Hort O., Dubrouil A., Cabasse A., Petit S., Mevel E., Descamps D., Constant E. *J. Opt. Soc. Am. B*, **32**, 1055 (2015).
142. Jacqmin H., Jullien A., Mercier B., Hanna M., Druon F., Papadopoulos D., Lopez-Martens R. *Opt. Lett*., **40**, 709 (2015).
143. Hädrich S., Kienel M., Müller M., Klenke A., Rothhardt J., Klas R., Gottschall T., Eidam T., Drozdy A., P. Jójárt, Várallyay Z., Cormier E., Osvay K., Tünnermann A., Limpert J. *Opt. Lett*., **41**, 4332 (2016).
144. Guo X., Tokita S., Yoshii K., Nishioka H., Kawanaka J. *Opt. Express*, **25**, 21171 (2017).
145. Lavenu L., Natile M., Guichard F., Zaouter Y., Hanna M., Mottay E., Georges P. *Opt. Express*, **25**, 7530 (2017).
146. Chen S., Jarnac A., Houard A., Liu Y., Arnold C.L., Zhou B., Forestier B., Prade B., Mysyrowicz A. *J. Opt. Soc. Am. B*, **28**, 1009 (2011).
147. Nagy T., Pervak V., Simon P. *Opt. Lett*., **36**, 4422 (2011).
148. Boehle F., Kretschmar M., Jullien A., Kovacs M., Miranda M., Romero R., Crespo H., Morgner U., Simon P., Lopez-Martens R., Nagy T. *Laser Phys. Lett*., **11**, 095401 (2014).
149. Cardin V., Thire N., Beaulieu S., Wanie V., Legare F.O., Schmidt B.E. *Appl. Phys. Lett*., **107**, 181101 (2015).
150. Jeong Y.-G., Piccoli R., Ferachou D., Cardin V., Chini M., Hädrich S., Limpert J., Morandotti R., Légaré F., Schmidt B.E., Razzari L. *Sci. Rep.*, **8**, 11794 (2018).
151. Chen B.-H., Kretschmar M., Ehberger D., Blumenstein A., Simon P., Baum P., Nagy T. *Opt. Express*, **26**, 3861 (2018).
152. Khodakovskiy N.G., Kalashnikov M.P., Pajer V., Blumenstein A., Simon P., Toktamis M.M., Lozano M., Mercier B., Cheng Z., Nagy T., Lopez-Martens R. *Laser Phys. Lett*., **16**, 095001 (2019).
153. Nagy T., Hadrich S., Simon P., Blumenstein A., Walther N., Klas R., Buldt J., Stark H., Breitkopf S., Jojart P., Seres I., Varallyay Z., Eidam T., Limpert J. *Optica*, **6**, 1423 (2019).
154. Ouillé M., Vernier A., Böhle F., Bocoum M., Jullien A., Lozano M., Rousseau J.-P., Cheng Z., Gustas D., Blumenstein A., Simon P., Haessler S., Faure J., Nagy T., Lopez-Martens R. *Light Sci. Appl*., **9**, 47 (2020).
155. Nagy T., Kretschmar M., Vrakking M.J.J., Rouzée A. *Opt. Lett*., **45**, 3313 (2020).
156. Beetar J.E., Nrisimhamurty M., Truong T.-C., Nagar G.C., Liu Y., Nesper J., Suarez O., Rivas F., Wu Y., Shim B., Chini M. *Sci. Adv.*, **6**, eabb5375 (2020).
157. Carpeggiani P.A., Coccia G., Fan G., Kaksis E., Pugžlys A., Baltuška A., Piccoli R., Jeong Y.-G., Rovere A., Morandotti R., Razzari L., Schmidt B.E., Voronin A.A., Zheltikov A.M. *Optica*, **7**, 1349 (2020).
158. Fan G., Carpeggiani P.A., Tao Z., Coccia G., Safaei R., Kaksis E., Pugzlys A., Légaré F., Schmidt B.E., Baltuška A. *Opt. Lett*., **46**, 896 (2021).
159. Nagy T., von Grafenstein L., Ueberschaer D., Griebner U. *Opt. Lett*., **46**, 3033 (2021).
160. Auguste T., Fourcade Dutin C., Dubrouil A., Gobert O., Hort O., Mével E., Petit S., Constant E., Descamps D. *Appl. Phys. B*, **111**, 75 (2013).
161. Nurhuda M., Suda A., Midorikawa K., Budiono H. *J. Opt. Soc. Am. B*, **22**, 1757 (2005).
162. Nurhuda M., Suda A., Midorikawa K., Hatayama M., Nagasaka K. *J. Opt. Soc. Am. B*, **20**, 2002 (2003).
163. Chen X., Jullien A., Malvache A., Canova L., Borot A., Trisorio A., Durfee C.G., Lopez-Martens R. *Opt. Lett*., **34**, 1588 (2009).
164. Nurhuda M., Suda A., Bohman S., Yamaguchi S., Midorikawa K. *Phys. Rev. Lett*., **97**, 153902 (2006).
165. Vlasov S.N., Koposova E.V., Yashin V.E. *Quantum Electron*., **42**, 989 (2012) [*Kvantovaya Elektron*., **42**, 989 (2012)].
166. Vysotina N.V., Rozanov N.N., Yashin V.E. *Opt. Spectrosc*., **110**, 973 (2011) [*Opt. Spectrosk*., **110**, 1029 (2011)].
167. Herriott D., Kogelnik H., Kompfner R. *Appl. Opt*., **3**, 523 (1964).
168. Sennaroglu A., Fujimoto J.G. *Opt. Express*, **11**, 1106 (2003).
169. Hanna M., Délen X., Lavenu L., Guichard F., Zaouter Y., Druon F., Georges P. *J. Opt. Soc. Am. B*, **34**, 1340 (2017).
170. Russbueldt P., Weitenberg J., Vernaleken A., Sartorius T., Schulte J. Patent No. US9847615B2 (2017).
171. Talanov V.I. *JETP Lett*., **11**, 199 (1970) [*Pis'ma Zh. Eksp. Teor. Fiz*., **11**, 303 (1970)].
172. Cao H., Nagymihaly R.S., Chvykov V., Khodakovskiy N., Kalashnikov M. *J. Opt. Soc. Am. B*, **36**, 2517 (2019).
173. Daher N., Guichard F., Jolly S.W., Délen X., Quéré F., Hanna M., Georges P. *J. Opt. Soc. Am. B*, **37**, 993 (2020).
174. Hanna M., Daniault L., Guichard F., Daher N., Délen X., Lopez-Martens R., Georges P. *OSA Contin.*, **4**, 732 (2021).
175. Cao H., Nagymihaly R.S., Kalashnikov M. *Opt. Lett*., **45**, 3240 (2020).
176. Schulte J., Sartorius T., Weitenberg J., Vernaleken A., Russbueldt P. *Opt. Lett*., **41**, 4511 (2016).
177. Weitenberg J., Vernaleken A., Schulte J., Ozawa A., Sartorius T., Pervak V., Hoffmann H.-D., Udem T., Russbüldt P., Hänsch T.W. *Opt. Express*, **25**, 20502 (2017).
178. Weitenberg J., Saule T., Schulte J., Rußbüldt P. *IEEE J. Quantum Electron*., **53**, 8600204 (2017).
179. Fritsch K., Poetzlberger M., Pervak V., Brons J., Pronin O. *Opt. Lett*., **43**, 4643 (2018).
180. Meyer F., Hekmat N., Vogel T., Omar A., Mansourzadeh S., Fobbe F., Hoffmann M., Wang Y., Saraceno C.J. *Opt. Express*, **27**, 30340 (2019).
181. Gröbmeyer S., Brons J., Seidel M., Pronin O. *Laser Photonics Rev*., **13**, 1800256 (2019).
182. Tsai C.-L., Meyer F., Omar A., Wang Y., Liang A.-Y., Lu C.-H., Hoffmann M., Yang S.-D., Saraceno C.J. *Opt. Lett*., **44**, 4115 (2019).
183. Meyer F., Vogel T., Ahmed S., Saraceno C.J. *Opt. Lett*., **45**, 2494 (2020).
184. Vicentini E., Wang Y., Gatti D., Gambetta A., Laporta P., Galzerano G., Curtis K., McEwan K., Howle C.R., Coluccelli N. *Opt. Express*, **28**, 4541 (2020).
185. Barbiero G., Wang H., Brons J., Chen B.-H., Pervak V., Fattahi H. *J. Phys. B: At. Mol. Opt. Phys.*, **53**, 125601 (2020).
186. Barbiero G., Wang H., Graßl M., Gröbmeyer S., Kimbaras D., Neuhaus M., Pervak V., Nubbemeyer T., Fattahi H., Kling M.F. *Opt. Lett.*, **46**, 5304 (2021).
187. Song J., Wang Z., Lv R., Wang X., Teng H., Zhu J., Wei Z. *Appl. Phys. B*, **127**, 50 (2021).
188. Ueffing M., Reiger S., Kaumanns M., Pervak V., Trubetskov M., Nubbemeyer T., Krausz F. *Opt. Lett*., **43**, 2070 (2018).
189. Lavenu L., Natile M., Guichard F., Zaouter Y., Delen X., Hanna M., Mottay E., Georges P. *Opt. Lett*., **43**, 2252 (2018).
190. Kaumanns M., Pervak V., Kormin D., Leshchenko V., Kessel A., Ueffing M., Chen Y., Nubbemeyer T. *Opt. Lett*., **43**, 5877 (2018).
191. Russbueldt P., Weitenberg J., Schulte J., Meyer R., Meinhardt C., Hoffmann H.D., Poprawe R. *Opt. Lett*., **44**, 5222 (2019).
192. Balla P., Wahid A.B., Sytcevich I., Guo C., Viotti A.-L., Silletti L., Cartella A., Alisauskas S., Tavakol H., Grosse-Wortmann U., Schönberg A., Seidel M., Trabattoni A., Manschwetus B., Lang T., Calegari F., Couairon A., L'Huillier A., Arnold C.L., Hartl I., Heyl C.M. *Opt. Lett*., **45**, 2572 (2020).
193. Grebing C., Müller M., Buldt J., Stark H., Limpert J. *Opt. Lett*., **45**, 6250 (2020).
194. Kramer Patrick L., Windeler Matthew K.R., Mecseki Katalin, Champenois Elio G., Hoffmann Matthias C., Tavella A.F. *Opt. Express*, **28**, 16951 (2020).
195. Kaumanns M., Kormin D., Nubbemeyer T., Pervak V., Karsch S. *Opt. Lett*., **46**, 929 (2021).
196. Müller M., Buldt J., Stark H., Grebing C., Limpert J. *Opt. Lett*., **46**, 2678 (2021).
197. Viotti A.-L., Alisauskas S., Bin Wahid A., Balla P., Schirmel N., Manschwetus B., Hartl I., Heyl C.M. *J. Synchrotron Radiat.*, **28**, 36 (2021).
198. Viotti A.-L., Alisauskas S., Tünnermann H., Escoto E., Seidel M., Dudde K., Manschwetus B., Hartl I., Heyl C.M. *Opt. Lett*., **46**, 4686 (2021).
199. Rueda P., Videla F., Witting T., Torchia G.A., Furch F.J. *Opt. Express*, **29**, 27004 (2021).
200. Daniault L., Cheng Z., Kaur J., Hergott J.-F., Réau F., Tcherbakoff O., Daher N., Délen X., Hanna M., Lopez-Martens R. *Opt. Lett*., **46**, 5264 (2021).
201. Kruglov V.I., Logvin Y.A., Volkov V.M. *J. Mod. Opt*., **39**, 2277 (1992).

202. Vuong L.T., Grow T.D., Ishaaya A., Gaeta A.L., Hooft G.W., Eliel E.R., Fibich G. *Phys. Rev. Lett*., **96**, 133901 (2006).
203. Lehmberg R.H., McMahon J.M. *Appl. Phys. Lett*., **28**, 204 (1976).
204. Petrov V., Rudolph W., Wilhelmi B. *J. Mod. Opt*., **36**, 587 (1989).
205. Mourou G., Cheriaux G., Radier C. Patent No. US20110299152A1 (2009).
206. Mironov S.Yu., Lozhkarev V.V., Khazanov E.A., Mourou G. *Quantum Electron*., **43**, 711 (2013) [*Kvantovaya Elektron*., **43**, 711 (2013)].
207. Mironov S., Khazanov E., Sergeev A.., Lassonde P., Kieffer J.-C., Mourou G. Patent No. US9678405 (2014).
208. Hunt J.T., Renard P.A., Nelson R.J. *Appl. Opt.*, **15**, 1458 (1976).
209. Perevezentsev E., Poteomkin A., Khazanov E. *Appl. Opt.*, **46**, 774 (2007).
210. Siegman A.E. *Proc. SPIE*, **1224**, 2 (1990).
211. Strehl K. *Z. Instrumentenkd*, **22**, 213 (1902).
212. Martyanov M., Mironov S., Starodubtsev M., Soloviev A., Kochetkov A., Ginzburg V., Shaykin A., Khazanov E., in *Proc. High-Brightness Sources and Light-Driven* (Interactions Congress, 23–25 March 2022, Budapest, Hungar, 2022) (to be published).
213. Mak A.A., Yashin V.E. *Opt. Spectrosc*., **70**, 1 (1991) [*Opt. Spectrosk*., **70**, 3 (1991)].
214. Andreev A.A., Mak A.A., Yashin V.E. *Quantum Electron*., **27**, 95 (1997) [*Kvantovaya Elektron*., **24**, 99 (1997)].
215. Mironov S.Y., Lozhkarev V.V., Ginzburg V.N., Yakovlev I.V., Luchinin G., Shaykin A.A., Khazanov E.A., Babin A.A., Novikov E., Fadeev S., Sergeev A.M., Mourou G.A. *IEEE J. Sel. Top. Quantum Electron*., **18**, 7 (2012).
216. Reitze D.H., Weiner A.M., Leaird D.E. *Opt. Lett*., **16**, 1409 (1991).
217. Mevel E., Tcherbakoff O., Salin F., Constant E. *J. Opt. Soc. Am. B*, **20**, 105 (2003).
218. Xiao-Fang L., Xiao-Wei C., Yong-Liang J., Jun L., Zhi-Nan Z., Ru-Xin L., Zhi-Zhan X. *Chinese Phys. Lett*., **23**, 3278 (2006).
219. Seidel M., Arisholm G., Brons J., Pervak V., Pronin O. *Opt. Express*, **24**, 9412 (2016).
220. He P., Liu Y., Zhao K., Teng H., He X., Huang P., Huang H., Zhong S., Jiang Y., Fang S., Hou X., Wei Z. *Opt. Lett*., **42**, 474 (2017).
221. Lu C.-H., Witting T., Husakou A., Vrakking M.J.J., Kung A.H., Furch F.J. *Opt. Express*, **26**, 8941 (2018).
222. Beetar J.E., Gholam-Mirzaei S., Chini M. *Appl. Phys. Lett*., **112**, 051102 (2018).
223. Lu C.-H., Wu W.-H., Kuo S.-H., Guo J.-Y., Chen M.-C., Yang S.-D., Kung A.H. *Opt. Express*, **27**, 15638 (2019).
224. Seo M., Tsendsuren K., Mitra S., Kling M., Kim D. *Opt. Lett*., **45**, 367 (2020).
225. Calendron A.-L., Meier J., Kueny E., Velten S., Bocklage L., Röhlsberger R., Kärtner F.X. *Appl. Opt.*, **60**, 912 (2021).
226. Stanfield M., Beier N.F., Hakimi S., Allison H., Farinella D., Hussein A.E., Tajima T., Dollar F. *Opt. Express*, **29**, 9123 (2021).
227. Krebs N., Pugliesi I., Riedle E. *Appl. Sci.*, **3**, 153 (2013).
228. Nkeck J.E., Guiramand L., Ropagnol X., Blanchard F. *J. Opt. Soc. Am. B*, **38**, 2715 (2021).
229. Rolland C., Corkum P.B. *J. Opt. Soc. Am. B*, **5**, 641 (1988).
230. Chvykov V., Radier C., Cheriaux G., Kalinchenko G., Yanovsky V., Mourou G. *Compression of Ultra-high Power Laser Pulses*, in *IEEE, 2010, OSA Techn. Digest (CD)* (Optica Publishing Group, 2010) paper JThG4.
231. Mironov S., Lassonde P., Kieffer J.C., Khazanov E., Mourou G. *Eur. Phys. J.: Spec. Top*., **223**, 1175 (2014).
232. Lassonde P., Mironov S., Fourmaux S., Payeur S., Khazanov E., Sergeev A., Kieffer J.C., Mourou G. *Laser Phys. Lett*., **13**, 075401 (2016).
233. Mironov S.Yu., Wheeler J., Gonin R., Cojocaru G., Ungureanu R., Banici R., Serbanescu M., Dabu R., Mourou G., Khazanov E.A. *Quantum Electron*., **47**, 173 (2017) [*Kvantovaya Elektron*., **47**, 173 (2017)].
234. Mironov S.Yu., Ginzburg V.N., Yakovlev I.V., Kochetkov A.A., Shaykin A.A., Khazanov E.A., Mourou G. *Quantum Electron*., **47**, 614 (2017) [*Kvantovaya Elektron*., **47**, 614 (2017)].
235. Lee S.K., Yoo J.Y., Kim J.I., Bhushan R., Kim Y.G., Yoon J.W., Lee H.W., Sung J.H., Nam C.H. *High Energy Pulse Compression by a Solid Medium*, in *Proc. Conference on Lasers and Electro-Optics (CLEO), San Jose, CA* (Optica Publishing Group, 2018) paper JTu2A.166.
236. Farinella D.M., Wheeler J., Hussein A.E., Nees J., Stanfield M., Beier N., Ma Y., Cojocaru G., Ungureanu R., Pittman M., Demailly J., Baynard E., Fabbri R., Masruri M., Secareanu R., Naziru A., Dabu R., Maksimchuk A., Krushelnick K., Ros D., Mourou G., Tajima T., Dollar F. *J. Opt. Soc. Am. B*, **36**, A28 (2019).
237. Masruri M., Wheeler J., Dancus I., Fabbri R., Nazîru A., Secareanu R., Ursescu D., Cojocaru G., Ungureanu R., Farinella D., Pittman M., Mironov S., Balascuta S., Doria D., Ros D., Dabu R. *Optical Thin Film Compression for Laser Induced Plasma Diagnostics*, in *Proc. Conference on Lasers and Electro-Optics (CLEO), San Jose, CA* (Optica Publishing Group, 2019) paper SW4E.3.
238. Ginzburg V.N., Yakovlev I.V., Zuev A.S., Korobeynikova A.P., Kochetkov A.A., Kuz'min A.A., Mironov S.Yu., Shaykin A.A., Shaikin I.A., Khazanov E.A. *Quantum Electron*., **49**, 299 (2019) [*Kvantovaya Elektron*., **49**, 299 (2019)].
239. Farinella D.M., Stanfield M., Beier N., Nguyen T., Hakimi S., Tajima T., Dollar F., Wheeler J., Mourou G. *Int. J. Mod. Phys. A*, **34**, 1943015 (2019).
240. Ginzburg V., Yakovlev I., Zuev A., Korobeynikova A., Kochetkov A., Kuzmin A., Mironov S., Shaykin A., Shaikin I., Khazanov E., Mourou G. *Phys. Rev. A*, **101**, 013829 (2020).
241. Ginzburg V.N., Yakovlev I.V., Zuev A.S., Korobeynikova A.P., Kochetkov A.A., Kuz'min A.A., Mironov S.Yu., Shaykin A.A., Shaikin I.A., Khazanov E.A. *Quantum Electron*., **50**, 331 (2020) [*Kvantovaya Elektron*., **50**, 331 (2020)].
242. Mironov S.Y., Fourmaux S., Lassonde P., Ginzburg V.N., Payeur S., Kieffer J.-C., Khazanov E.A., Mourou G. *Appl. Phys. Lett*., **116**, 241101 (2020).
243. Tamer I., Hornung M., Lukas L., Hellwing M., Keppler S., van Hull R., Hein J., Zepf M., Kaluza M.C. *Opt. Lett*., **45**, 6575 (2020).
244. Ginzburg V., Yakovlev I., Kochetkov A., Kuzmin A., Mironov S., Shaikin I., Shaykin A., Khazanov E. *Opt. Express*, **29**, 28297 (2021).
245. Shaykin A., Ginzburg V., Yakovlev I., Kochetkov A., Kuzmin A., Mironov S., Shaikin I., Stukachev S., Lozhkarev V., Prokhorov A., Khazanov E. *High Power Laser Sci. Eng*., **9**, 7 (2021).
246. Kieffer J.C., Ham B., Hallin E., Brereton N., Fourmaux S., Lassonde P., Mironov S.Y., Khazanov E.A., Mourou G., in *Proc. High-Brightness Sources and Light-Driven Interactions Congress* (23–25 March 2022, Budapest, Hungar) (to be published).
247. Vlasov S.N., Petrishchev V.A., Talanov V.I. *Radiophys. Quantum Electron*., **13**, 908 (1970) [*Izv. Vyssh. Uchebn. Zaved., Ser. Radiofiz*., **13**, 908 (1970)].
248. Centurion M., Porter M.A., Kevrekidis P.G., Psaltis D. *Phys. Rev. Lett*., **97**, 033903 (2006).
249. Bergé L., Mezentsev V.K., Rasmussen J. Juul, Christiansen P. Leth, Gaididei Y.B. *Opt. Lett*., **25**, 1037 (2000).
250. Lu C.-H., Tsou Y.-J., Chen H.-Y., Chen B.-H., Cheng Y.-C., Yang S.-D., Chen M.-C., Hsu C.-C., Kung A.H. *Optica*, **1**, 400 (2014).
251. Cheng Y.-C., Lu C.-H., Lin Y.-Y., Kung A.H. *Opt. Express*, **24**, 7224 (2016).
252. Ginzburg V.N., Kochetkov A.A., Yakovlev I.V., Mironov S.Yu., Shaykin A.A., Khazanov E.A. *Quantum Electron*., **46**, 106 (2016) [*Kvantovaya Elektron*., **46**, 106 (2016)].
253. Chilingaryan Yu.S. *Sov. Phys. JETP*, **28**, 832 (1969) [*Zh. Eksp. Teor. Fiz*., **55**, 1589 (1968)].
254. Ginzburg V.N., Kochetkov A.A., Mironov S.Yu., Potemkin A.K., Silin D.E., Khazanov E.A. Radiophys. *Quantum Electron*., **62**, 849 (2020) [*Izv. Vyssh. Uchebn. Zaved., Ser. Radiofiz*., **62**, 953 (2019)].
255. Mironov S., Lozhkarev V., Luchinin G., Shaykin A., Khazanov E. *Appl. Phys. B: Lasers Opt.*, **113**, 147 (2013).
256. Ginzburg V.N., Kochetkov A.A., Poteomkin A.K., Khazanov E.A. *Quantum Electron*., **48**, 325 (2018) [*Kvantovaya Electron*., **48**, 325 (2018)].
257. Kochetkova M.S., Martyanov M.A., Potemkin A.K., Khazanov E.A. *Quantum Electron*., **39**, 923 (2009) [K*vantovaya Elektron*., **39**, 923 (2009)].
258. Rajaofara Z., Leproux P., Capitaine E., Kano H., Hayakawa T., Thomas P., Duclère J.-R., Couderc V. *AIP Adv.*, **9**, 105301 (2019).
259. Mironov S., Gacheva E., Ginzburg V., Silin D.E., Kochetkov A., Mamaev Y., Shaykin A., Khazanov E., Mourou G. *Laser Phys. Lett*., **12**, 025301 (2015).

260. Vlasov S.N. *Sov. J. Quantum Electron*., **6**, 245 (1976) [*Kvantovaya Elektron*., **3**, 451 (1976)].
261. Baranova N.B., Bykovsky N.E., Senatsky Yu.V., Chekalin S.V. *J. Sov. Laser Research*, **1**, 62 (1980) [*Trudy FIAN*, **103**, 84 (1978)].
262. Bykovsky N.E., Ivanov V.V., Senatsky Yu.V. *Trudy FIAN*, **149**, 150 (1985).
263. Baranova N.B., Bykovsky N.E., Zeldovich B.Ya., Senatsky Yu.V. *Sov. J. Quantum Electron*., **4**, 1362 (1974) [*Kvantovaya Elektron*., **1**, 2450 (1974)].
264. Babichenko S.M., Bykovsky N.E., Senatsky Yu.V. *Sov. J. Quantum Electron*., **12**, 105 (1982) [*Kvantovaya Elektron*., **9**, 161 (1982)].
265. Mironov S.Y., Wheeler J.A., Khazanov E.A., Mourou G.A. *Opt. Lett*., **46**, 4570 (2021).